THESIS

GEOGRAPHICALLY-RESOLVED EVALUATION OF THE ECONOMIC AND ENVIRONMENTAL SERVICES FROM RENEWABLE DIESEL DERIVED FROM ATTACHED ALGAE FLOW-WAYS ACROSS THE UNITED STATES

Submitted by

Austin Brice Banks

Department of Mechanical Engineering

In partial fulfillment of the requirements

For the Degree of Master of Science

Colorado State University

Fort Collins, Colorado

Summer 2022

Master's Committee:

Advisor: Jason Quinn

Christie Peebles
Bret Windom

ABSTRACT

GEOGRAPHICALLY-RESOLVED EVALUATION OF THE ECONOMIC AND ENVIRONMENTAL SERVICES FROM RENEWABLE DIESEL DERIVED FROM ATTACHED ALGAE FLOW-WAYS ACROSS THE UNITED STATES

Harmful algal blooms (HABs) are becoming more invasive and ever more prevalent due to rises in nitrogen and phosphorus pollution in watersheds. Nitrogen and phosphorus leakages primarily occur from non-point sources like agricultural runoff, but also point sources like wastewater treatment facilities. Previous efforts to reduce nitrogen and phosphorus loadings and mitigate HABs have largely been ineffective despite investment in nutrient reduction technologies. As the population grows, our consumption and dispersal of nitrogen and phosphorus is expected to compound, and HABs will continue to wreak havoc on our aquatic ecosystems. Herein, we introduce a novel biorefinery that taps into the vast sources of nitrogen and phosphorus in watersheds while simultaneously producing biofuels. Contaminated water is diverted to flow over attached algae systems, feeding native, periphytic algal cultures and scrubbing excessive nutrients from the water. Hydrothermal liquefaction converts the algal biomass into renewable fuels, nutrient-rich fertilizers, and carbonaceous char. The evaluation of the biorefinery concept is done through integrating geographically-resolved growth modeling with nutrient resource availability based on all Hydrologic Unit Code-8 (HUC8) in the contiguous US which is integrated into sustainability models to evaluate the economic and environmental impact of the proposed system. Life cycle analysis results demonstrate a global warming potential of 25 g $CO_{2\text{-eq}}$ MJ^{-1}, a eutrophication potential of $1.3*10^{-5}$ kg N eq MJ^{-1} , and

a net energy ratio 0.33 of MJ MJ^{-1} in the Santa Monica Bay, CA subbasin. Technoeconomic assessments found that renewable diesel can be produced for $1.20 per cubic decimeter (dm^{-3}) or $4.56 per gallon of gasoline equivalent (GGE^{-1}) under optimal conditions in the Santa Monica Bay, CA subbasin, with results dramatically varying across the US. Water quality trading was also incorporated into the analysis. Using modest nutrient credit values of $4.5 per kg of total nitrogen ($kg\text{-}TN^{-1}$) and $4.5 per kg total phosphorus ($kg\text{-}TP^{-1}$) removed enabled the renewable diesel to achieve parity with conventional diesel, $1.01 dm^{-3} ($3.84 GGE^{-1}) in the Santa Monica Bay, CA subbasin. A more aggressive credit value of $45 $kg\text{-}TN^{-1}$ and $45 $kg\text{-}TP^{-1}$ made the price of the renewable diesel negative in Santa Monica Bay, CA, roughly $-4.45 dm^{-3} ($-16.8 GGE^{-1}), and across the Midwest, the Gulf of Mexico, and major cities on the East and West Coast. This means the value of the service that the algae provide in remediating watersheds covers all costs of the system to the point where the renewable diesel represents a product with negligible value. These results highlight a path forward for mitigating eutrophication while also creating a sustainable fuel. Discussion focuses on the service that large-scale deployment of attached algae flow-ways provide to remediate excessive nutrients from watersheds and generate biofuels at a cost-effective price point when water quality trading credits are incorporated into the system economics.

TABLE OF CONTENTS

ABSTRACT ii
Chapter 1 - Introduction 1
1.1 Background 1
Chapter 2 – Methodology 5
2.1 Introduction 5
2.2. Geographically resolved input data 6
2.2.1. Water quality data 6
2.2.2. Typical meteorological year data 7
2.2.3. Operational days data 7
2.3. Algae production with an attached algae flow-way 7
2.3.1. Nutrient reduction 8
2.3.2. 1st order growth model 8
2.2.3. Attached algae flow-way scaling 9
2.4. Biofuel conversion 12
2.4.1. Algae pretreatment 12
2.4.2. Hydrothermal liquefaction 12
2.4.3. Biocrude upgrading 13
2.5. Life cycle analysis 14
2.6. Techno-economic assessment 15
2.7. Sensitivity analysis 17
2.8. Water quality trading 17
Chapter 3 – Results and discussion 19
3.1. Introduction 19
3.2. Baseline life cycle analysis 19
3.2.1. Global warming potential (100-year horizon) 20
3.2.2. Eutrophication 21
3.2.3. Net energy ratio 22
3.2.4. Acidification 22
3.2.5. Ecotoxicity 23
3.2.6. Human health (carcinogenic and non-carcinogenic) 23
3.2.7. Ozone depletion 24
3.2.8. Photochemical ozone formation 24
3.2.9. Fossil fuel depletion 25
3.2.10. Respiratory effects 25
3.2.11. Life cycle analysis interpretation 26
3.3. Baseline techno-economic assessment 27
3.4. Baseline sensitivity analysis 32
3.5. HUC8 model results 36
3.5.1. HUC8 model techno-economic assessment 37
3.5.2. HUC8 model water quality trading 42

Chapter 4 – Conclusions 46
Bibliography 48
Appendix A 56
1. Water quality data 56
2. Operational days data 59
3. 1st order algae growth model 60
4. Variable algae composition 64
5. Life cycle analysis 66
6. Bioenergy Technology Office cost assumptions 68
7. Cost estimates 68
8. Bibliography 71

Chapter 1 - Introduction

1.1 Background

Algal blooms are a natural component to seasonal cycles of temperate lakes and oceans by driving zooplankton production, a critical source of food for aquatic ecosystems [1]. However in recent decades, large accumulations of phytoplankton and macroalgae have been reported globally, giving rise to red or green tides that cover beaches with decaying biomass, deplete dissolved oxygen levels critical to fisheries and wildlife, and in some cases, excrete toxins [2]. These accumulations are known as harmful algal blooms (HABs) and are typically the result of elevated nutrient loadings [3]. Excess nitrogen and phosphorus from agriculture runoff, animal manure, storm water, and wastewater leech into watersheds where they cause eutrophication and lead to the formation of HABs [2,4–7]. HABs are found inside all 50 states and along every major coastline of the US [8–12]. Failure to reduce nutrient loads not only enables the destruction of aquatic ecosystems, but also results in billions of dollars of economic damages [13]. Losses in tourism, property values, seafood sales, and mitigation costs are direct consequences of HABs with a need to identify cost effective ways for mitigating excess nutrients [14,15].

Nutrient reduction technologies exist to proactively curtail nitrogen and phosphorus loadings into surface waters. Wastewater treatment facilities have incorporated advanced water treatment technologies to meet more stringent effluent concentrations [16], but their high costs will likely prohibit their installation en masse for dilute nutrient remediation. Best management practices (BMPs) have also been utilized to address nutrient pollution on agricultural land, but HABs continue to persist despite considerable investment in these programs [17,18]. Fewer

farmers than expected have participated in BMP programs due to their voluntary nature [19]. Cover crops, for example, are only utilized on 5% of all US cropland [19]. This calls into question the effectiveness of these nutrient reduction technologies if no incentive structures exist or no other co-benefits are realized. There is a need for alternative mitigation technologies to address the impact of dilute nutrients in various watersheds.

Attached algae flow-ways are an effective tool for surface water remediation of dilute nutrients [15], [20–24]. In such systems, surface waters contaminated with excess nitrogen and phosphorus are diverted and surged over a flow way that contains an algal substrate. Native, filamentous algae (i.e. periphyton) utilize the substrate as a habitat for attachment, growth, and proliferation as they employ nutrients for photosynthetic metabolism. The flow rate of the system is controlled to maintain enough contact between the contaminated water and the algae to ensure the removal of nutrients before the water is reintroduced to the environment. The algae are harvested periodically to ensure biomass is produced continuously and water remediation is unimpeded. Not only are attached algae flow-ways able to remove nitrogen and phosphorus upstream so that nutrients cannot accumulate downstream, but they also produce a valuable biomass co-product which can be a feedstock for biorefining concepts.

Biofuels are one of the many potential uses from the biomass co-product. Algae biofuels have long been touted as the future of renewable fuels because they can be cultivated on non-arable land, are capable of being integrated with waste streams, and do not compete for food resources [25–28]. Algae biofuels have also been demonstrated to have a lower carbon footprint than conventional fuels because they remove CO_2 from the air [29]. As impacts of global warming continue to mount, transitioning to sustainable fuels is imperative. However, the price of biomass production is often cited as the prohibiting factor in algal systems [30–32]. Further,

traditional cultivation techniques rely on external inputs of nutrients to sustain growth, which seems counterproductive in the context of a looming phosphorus shortage [33]. If global dependence on fossil fuels is to be phased out, the focus needs to be shifted from viewing algae only as a product to valuing the services it provides and capitalize on nature's solution for dealing with excessive nutrient pollution.

Attached algae flow-ways are an application of biomimicry because they resemble accumulations of native algal species that thrive in nutrient-rich water [34]. Previous site-specific studies have assessed the ability of attached algae flow-ways to remove excess nutrients from waterways [20,21,23,24,35,36]. Others have assessed the economic feasibility of producing biofuels from the biomass [22,30,32,37]. System improvements that would improve the value of the biomass for biobased commodity applications, like ash reduction has also been studied in great detail [38]. While these studies treat the algae as a product, some studies have implored the potential services of attached algae flow-ways to proactively mitigate HABs [15]. This work builds upon previous studies and identifies a path forward by unlocking the potential of attached algae flow-ways through a valuation of the environmental services of algae cultivation with impaired surface waters.

The fact that HABs form in runoff-impacted surface waters demonstrates that algae are a potential solution to the problem, but only if the biomass can be easily recovered from the water without further disturbance to the ecosystem. This work investigates the economic and environmental feasibility of deploying attached algae flow-ways to clean watersheds, while also creating renewable diesel. A national resource assessment of nutrient removal with attached algae flow-ways is conducted through a geographically-resolved algae growth model coupled with a biorefining model. Water quality data was obtained to understand nutrient loads at the

subbasin-level. Algae production was predicted through nutrient load reductions required to meet water quality standards and by the determination of a local, annual average algae productivity. Subsequent renewable diesel production through hydrothermal liquefaction (HTL) was modeled by simulating the material and energy balances. The environmental and economic viability of the biorefinery concept considering geographically-resolved nutrient and weather data was completed. Discussions from this study not only highlights algal biomass sourced from attached algae flow-ways can aid in the remediation of waterways impaired by excessive nutrient pollution, but also the importance of incorporating water quality trading into the economic analysis to enable wide-spread adoption of attached algae biofuel systems.

Chapter 2 – Methodology

2.1 Introduction

A process model of algae production based on an attached algae flow-way and subsequent biofuel conversion through HTL was created from the design considerations from recent studies [15,24,32,39–41]. Water quality data, weather data and operational days data served as inputs to the process model that enabled geographic resolution at the Hydrologic Unit Code 8-Digit (HUC8) scale [42–49]. Excel spreadsheets aided in the development of material and energy balance simulations for the unit operations contained within the system boundary. The weather and nutrient load datasets and biorefinery process model can be found in Appendix A. Results from the process model informed environmental and economic assessments utilizing a well-to-wheel system boundary. The life cycle analysis (LCA) determined the net energy ratio and the environmental impact based on the ten impact categories found in the Tool for the Reduction and Assessment of Chemical and Other Environmental Impacts (TRACI) version 2.1 for the system. The techno economic assessment (TEA) leveraged model outputs and economic assumptions to determine the minimum fuel selling price of the renewable diesel. The feasibility of the system was further evaluated with the addition of water quality trading. A process flow diagram of the biorefinery system is displayed in Fig. 1.

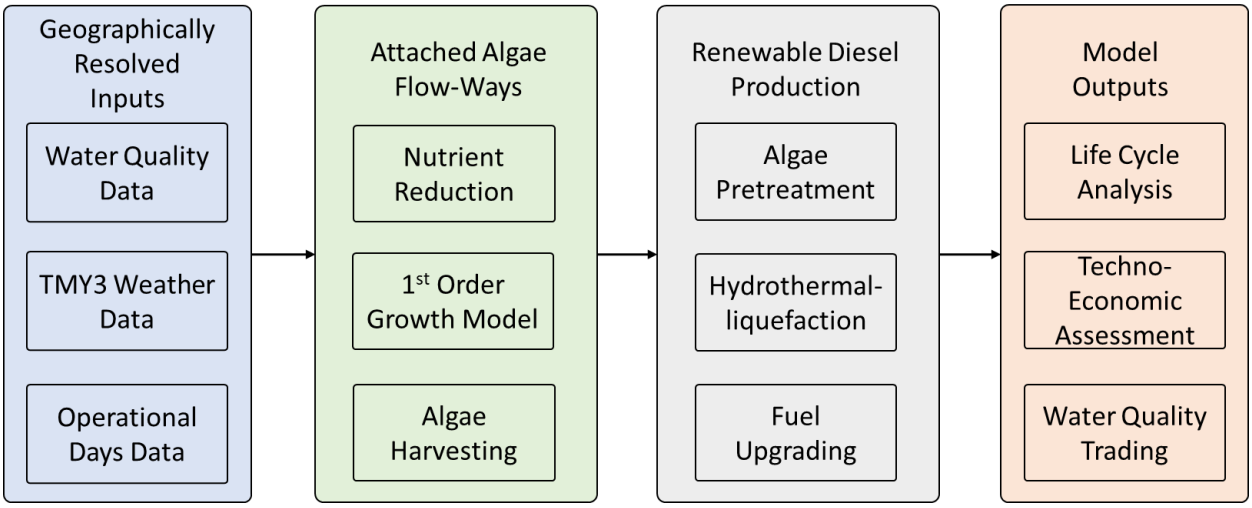

Fig. 1. Process flow diagram for removing nutrients from waterways via attached algae flow-ways. The algae is then converted to renewable diesel. Life cycle and techno-economic assessments evaluated the effectiveness of the proposed biorefinery.

2.2. Geographically resolved input data

Geographically resolved data for weather and water quality were obtained and represent core inputs to the modeling work. Weather data was used to extrapolate a geographically-resolved algae growth model which was calibrated from algae growth data from a field trial. Water quality data was used to estimate nutrient loads across the US.

2.2.1. Water quality data

Water quality data served as the foundation for assessing the degree to which watersheds were impaired from excessive nutrients and where algal systems could be deployed. Watersheds exist on a variety of scales and there are tradeoffs in data resolution and model output uncertainty depending on the scale used [50]. This study identified impairment within the 2,112 HUC8 subbasins in the contiguous US. The U.S. Geological survey released a suite of reports on the five major water regions that contain these HUC8 subbasins [42–46]. These reports detail mean annual streamflow, total nitrogen, total phosphorus, and suspended sediment loads from agriculture, wastewater treatment and other sources in the watersheds. It should be noted that

Southern Florida was excluded from the data set due to inability to accurately predict nutrient loadings in that region [42]. Total nitrogen (TN) and total phosphorus (TP) concentrations were calculated from the delivered aggregate loads from all sources, which enabled nutrient load reduction calculations at the HUC8 level.

2.2.2. Typical meteorological year data

Regional weather data was obtain from the Typical Meteorological Year (TMY3) data set [47]. Using a similar methodology employed by Greene et al (2021) and Beattie et al (2021), annual average global horizontal irradiance (GHI) data were mapped to each HUC8 [48,51]. The GHI at individual HUC8 subbasins were found by finding the minimum distance of the HUC8 centroid to the nearest TMY3 monitoring station. It was assumed that the GHI each HUC8 received in a typical year were constant, translating to a unique annual average GHI for each HUC8 subbasin. The TMY3 data allowed for the calibration and extrapolation of a 1st order growth model and estimations of algae productivities at the HUC8-level.

2.2.3. Operational days data

Operational days data were utilized to facilitate ambient temperature effects on algae growth. Previous work from Quiroz et al. (2021) informed the modeling framework to determine the operational days for each HUC8 [49]. The data accounts for the number of freezing events in open algae cultivation systems and is based on real temperature data. It was assumed that an attached algae flow-way operates for the remainder of the days in a year that did not experience a freezing event.

2.3. Algae production with an attached algae flow-way

A 1st order algae growth model was developed from field data acquired by Sandia National Laboratories in Corpus Christi, TX [24]. The functional growth model was then applied

to each HUC8 utilizing water quality and weather data. The attached algae flow-ways were sized according to the load reductions required to meet defined effluent TN and TP concentrations. Algae production was predicted, and the resulting size of the attached algae flow-ways was determined. Further description of the design considerations for the attached algae flow-ways are contained in the following sections.

2.3.1. Nutrient reduction

Nutrient reduction for the flow-ways were met by specifying a target effluent concentration as the criteria of success in this study. Specifying the target concentration of nutrients enables a direct evaluation of the impaired waters in relation to compliance criteria set by a total maximum daily load (TMDL). TMDLs were established under the Clean Water Act of 1972 to address the maximum amount of pollutant a source can emit to ensure water quality standards are met [52]. TMDL frameworks serve as the starting point for addressing remediation. The EPA offers guidelines for local authorities to issue permits that establish TMDLs for point and non-point source emitters [53]. The permits take local ecosystems and community stakeholder goals into account, which causes water quality targets to vary between cities, counties, and states. Based on the limits established by some states [54–57], target effluent limits for nitrogen and phosphorus were set to 1.0 mg-TN L^{-1} and 0.1 mg-TP L^{-1}, respectively.

2.3.2. 1st order growth model

The algae growth model estimates annual average productivities as a function of light input through determination of a photosynthetic light efficiency [58]. To determine the base-case photosynthetic efficiency, the 1st order growth model was validated with productivity data from Sandia National Laboratories and the corresponding TMY3 weather data from Laguna Madre, TX [24]. During 6 months of the field trial, the attached algae flow-way demonstrated an annual

average productivity of 9.6 g m^{-2} day^{-1}, which translates to a photosynthetic light efficiency of 1.4%. The data from Sandia National Laboratories and the equation used in this calculation can be found in Appendix A. Leveraging TMY3 data across the US allowed for local annual average productivities to be calculated at each subbasin by assuming a constant light efficiency. The US maximum annual productivity for a light efficiency of 1.4% was 12.4 g m^{-2} day^{-1}. Two additional productivities were forecasted for the attached algae flow-ways.

Recent data generated at the Sandia Algae Testbed shows that it is possible to achieve an increased productivity with grow lights under controlled conditions. It was assumed a maximum annual productivity of 25 g m^{-2} day^{-1} in the US occurs where the local annual average GHI is the greatest, which conservatively predicts this near-term productivity projection for the attached algae flow-ways. For example, a maximum annual productivity was achieved in southwestern New Mexico near Gila National Forest. Lastly, a best-case productivity was identified as 40 g m^{-2} day^{-1} and is consistent with projections for other algae cultivation systems [59]. The light efficiencies were then back-calculated with TMY3 data from New Mexico and were found to be 2.8% for 25 g m^{-2} day^{-1} and 4.5% for 40 g m^{-2} day^{-1}. These light efficiencies were all assumed to be constant, allowing for the local annual average productivities to be calculated from the local annual average GHI.

2.2.3. Attached algae flow-way scaling

The Redfield ratio is also an important metric to consider when deploying attached algae flow-ways. Aquatic organisms like phytoplankton typically uptake nitrogen and phosphorus in a ratio of 16:1 [60]. This ratio, the Redfield ratio, helps reference nutrient limitations for biomass growth [61]. In this study, attached algae flow-ways were sized to treat the limiting nutrient, relative to the nitrogen to phosphorus (N:P) ratio of algae harvested from the attached algae

flow-ways, to the specified effluent limit. This decision helps to prevent oversizing of the attached algae flow-ways and conservatively predict where deployment is feasible to stakeholders.

Field trails from Sandia National Laboratories have shown that attached algae flow-ways can adapt to varying inflow nutrient ratios and exist with N:P ratios ranging from 13:1 to 86:1 with different elemental compositions at both bounds (**Error! Reference source not found.**). To a ddress this, a variable composition calculation was introduced to the model that ensured the algae N:P ratio was equivalent to the inflow TN:TP ratio within the bounds of the known compositions. It was assumed that if the inflow TN:TP ratio is less than 13:1, the system is nitrogen limiting (N-limiting) and the nitrogen and phosphorus compositions were based on the nitrogen-limiting algae composition. Whereas, if the inflow TN:TP ratio is greater than 86:1, the system is severely phosphorus limiting (P-limiting), thus the nitrogen and phosphorus compositions were based on the phosphorus-limiting algae composition. For inflow TN:TP ratios between the two bounds, the system is still phosphorus limiting, but in this case the nitrogen and phosphorus compositions were calculated to ensure that the algae N:P ratio was equivalent to the inflow TN:TP ratio. More details about how the variable compositions can be found in Appendix A.

Table 1. Elemental composition of algae harvested from an attached algae flow-way for inflow TN:TP ratios of 13:1 and 86:1 (mol mol^{-1}).

Element	**N-limiting Composition (wt%)**	**P-limiting Composition (wt%)**
C	37.7%	43.9%
H	7.9%	7.1%
O	48.2%	40.8%
N	5.3%	8.0%
P	0.9%	0.2%

N:P ratio	13:1	86:1

After estimating the local productivity and algae composition, the size of the attached algae flow-way module can be determined. Based on the assumption that the inflow TN:TP ratio is equivalent to the algae N:P ratio, it is impossible for both effluent limits to be met unless the inflow TN concentration is an order of magnitude greater than the inflow TP concentration (i.e. 2.0 mg-TN L^{-1} and 0.2 mg-TP L^{-1}) since the target effluent limits are also different by an order of magnitude. The module areas were calculated by first determining the theoretical load reductions required to meet both target effluent limits (1.0 mg-TN L^{-1} and 0.1 mg-TP L^{-1}). Then, the actual TN and TP load reductions were selected based on inflow N:P ratio. If the inflow TN:TP ratio is N-limiting, then the actual TN load reduction is equal to the theoretical TN load reduction and the actual TP reduction is scaled from the N-limiting algae N:P ratio. Conversely, if the inflow TN:TP ratio is severely P-limiting, then the actual TP load reduction is equal to the theoretical TP load reduction and the actual TN load reduction is scaled from the P-limiting algae N:P ratio. For inflow TN:TP ratios in between the two bounds, the actual TP load reduction is equal to the theoretical TP load reduction and the actual TN load reduction is scaled from the variable algae N:P ratio. The area required for treatment was then found with the following equation:

$$N - limiting\ Area\ [m^2] = \frac{\Delta TN}{x_N * P}$$

Where ΔTN is the actual TN load reduction (g day^{-1}), x_N is the mass fraction of nitrogen in the algae biomass, and P is the algae productivity (g m^{-2} day^{-1}). The P-limiting area can be calculated by substituting in the corresponding phosphorus values, however, the logic from the previous calculations ensures that the P-limiting area is equivalent to the N-limiting area because

the actual nutrient reductions and algae compositions were calculated from the algae N:P ratio. Finally, the algae production can be found by multiplying the area by the algae productivity.

2.4. Biofuel conversion

This work models a thermochemical conversion through HTL, which converts a wet feedstock into biocrude under high temperatures and pressures [27]. In addition to the biocrude, a three phase mixture is also present in the effluent of the HTL reactor: a solid biochar phase, an aqueous organic phase, and a non-condensable gas phase. The co-products are separated and refined into compost, concentrated fertilizer, and supplemental heating from the off gases.

2.4.1. Algae pretreatment

After harvesting the algae biomass, pretreatment was required to reduce the ash content. Although attached algae systems can have ash content >50 wt%, experimental data from Sandia National Laboratories has demonstrated that ash content of 15-20 wt% is feasible from long-term (6 months continuous) cultivation. This study assumed post-harvest ash content was 20wt% solids. A simple water wash was employed to further reduce the ash content by 45wt% with minimal biomass loss (1wt%) over the course of 24 hours [15], [38]. A filter press reduced the final slurry concentration of the algae feed to 20wt% solids prior to conversion in the HTL system [38].

2.4.2. Hydrothermal liquefaction

The HTL process model was based on the design considerations found in Chen et al. (2021) [39]. Algae biomass is thermochemically treated in subcritical water at 20.7 MPa (3,000 psia) and 350°C. The reaction yields (on an AFDW basis) for the biocrude, aqueous organics, gas, and char were assumed to be 45 wt%, 40 wt%, 13 wt%, and 2 wt%, respectively [39]. After the reaction, a gas knock-out drum removed the non-condensable gases from the mixture, which

helped to supplement the fuel requirements for process heating. The char was then separated with a solids filter and sent to solids disposal [59]. A two-phase separator recovered the biocrude from the aqueous organics and continued to fuel upgrading. The aqueous organics were pumped through heat exchangers to alleviate feed preheater energy requirements. Although energy was recovered from co-products, oil for process heating was needed to raise the temperature of the feed to the reaction temperature. The hot oil heat exchanger energy requirement (1,420 kJ per kg AFDW biomass) was met with supplemental natural gas.

2.4.3. Biocrude upgrading

HTL biocrude requires upgrading before it can be used as a drop-in fuel replacement. Removing nitrogen, oxygen, and sulfur contaminants from the biocrude improves the efficiency of the fuel and reduces emissions of harmful combustion products like NO_x and SO_x [59]. Compressed hydrogen (4.3 wt%) was reacted with the biocrude in the hydrotreater to remove the fuel contaminants. Off gases were recycled to the hot oil heater to further supplement process heating requirements. The hydrogen duty for the upgrading was met by purchasing hydrogen. Of the biocrude entering the hydrotreater, 59 wt% was upgraded to diesel, 10 wt% was upgraded to naphtha, and 8.4 wt% was recovered as heavy oil. The diesel and naphtha were separated from the heavy oil in a series of distillation columns, and the heavy oil was further refined in a hydrocracker. The hydrotreating system resulted in energy requirements of 145 kJ (kg biocrude)$^{-1}$ of electricity, 1080 kJ (kg biocrude)$^{-1}$ of natural gas, and 457 kJ (kg biocrude)$^{-1}$ of cooling water.

Long-chain hydrocarbons in the heavy oil were upgraded in the hydrocracker to produce more diesel and naphtha. The heavy oil reacted with compressed hydrogen (2.0 wt%) and yielded 59 wt% diesel and 27 wt% naphtha. The diesel and naphtha from the hydrotreater and

the hydrocracker were stored in tanks with a 3-day holding capacity before being sold. The energy requirements from the hydrocracker were 212 kJ (kg heavy oil)$^{-1}$ of electricity, 470 kJ (kg heavy oil)$^{-1}$ of natural gas, and 602 kJ (kg heavy oil)$^{-1}$ of cooling water.

2.5. Life cycle analysis

The baseline LCA was conducted at one of the HUC8 subbasins, Santa Monica Bay, CA. This location was chosen because it is adjacent to one of the most populated metropolitan areas in the US [62] and suffers from a 'red tide' HAB nearly every year. Santa Monica Bay, CA is a potential deployment location for attached algae flow-ways due to its large population, high nutrient loadings and optimal weather conditions that are conducive for algae growth, despite potential issues with land availability. The environmental impacts from remediating the subbasin with an attached algae flow-way and producing biofuels are assessed.

The goal of this attributional LCA is to quantify the environmental impacts of renewable diesel relative to conventional diesel. A functional unit of 1 MJ fuel produced was used to facilitate this analysis. The system boundary for the LCA is like the TEA system boundary, but it is expanded to include the end use of the renewable diesel, known as a well-to-wheels (WTW) system boundary. The fuel end use contributions were determined with low-sulfur diesel (75 g CO_2 eq MJ^{-1}) [63]. The attached algae flow-way was assumed to be co-located with the pretreatment, conversion and upgrading processes found inside the HTL facility. Nutrient recycling to the algal cultivation system was not considered as in Chen et al. (2021), but instead a nutrient credit was generated for removing bioavailable nitrogen and phosphorus from the water and displacing NH_3 and $(NH_4)_2HPO4$ fertilizer [39]. Direct Land Use Change was not considered [39].

Life cycle inventory (LCI) data were acquired primarily from the *ecoinvent Version 3.4* database in the openLCA software with product flows and impacts determined with the "cutoff" method [64,65]. Since the study location is in California, the WECC grid mix, high voltage process was selected as the electricity source. Hydrogen LCI data were obtained from natural gas steam reforming LCA [66]. Recovered nitrogen and phosphorus displaced NH_3 and diammonium phosphate (DAP) fertilizer [64]. The TRACI 2.1 methodology aided in quantifying the environmental impacts and employs ten impact categories: acidification, ecotoxicity, eutrophication, global warming (100-year horizon), human health (carcinogenic and non-carcinogenic), ozone depletion, photochemical ozone formation, resource depletion, and respiratory impacts. Net energy ratio (NER) was also included in this LCA study, which is defined as the ratio of the energy inputs to the energy outputs. Impacts from the renewable diesel were compared with conventional, low-sulfur diesel on a WTW system boundary.

2.6. Techno-economic assessment

The baseline TEA was conducted at Santa Monica Bay, CA and two additional locations (Buffalo-San Jacinto, TX and Sandusky, OH) were included in the baseline TEA study. Buffalo-San Jacinto, TX is a subbasin located within Houston, TX and experiences high nutrient loadings from urban land and municipal wastewater treatment discharge [46]. The Sandusky, OH subbasin is located in a major agricultural region and suffers from nutrient discharges predominantly occurring from agricultural runoff [44]. These three locations serve as a foundational locations for the capabilities of this biorefinery in both urban and rural environments. After proving the baseline model, the system was then applied to all HUC8 subbasins in the contiguous US.

A discounted cash flow rate of return model was utilized to determine the minimum biomass selling price (MBSP) and the minimum fuel selling price (MFSP). The "N^{th}-of-a-kind" plant economic assumptions, as outline by the Bioenergy Technologies Office (BETO) were assumed [41]. These include an internal rate of return of 10%, a 60:40 plant debt to equity financing, and a debt financing term of 10 years at an interest rate of 8%. A complete list of the "N^{th}-of-a-kind" plant assumptions is found in Appendix A. Inputs and outputs from the process model inform the capital expenses (CAPEX) and the operational expenses (OPEX). These expenses are then fed into the economic model where the values of the product revenues are determined to ensure a net present value of zero for the lifetime of the plant. Similar to Chen et al. (2021), all liquid fuels were lumped together to determine their price on a cubic decimeter of gasoline equivalent basis or a gallon of gasoline equivalent basis [39].

Cost estimation for the attached algae flow-ways were based on a previous study from DeRose et al. (2021) [15]. These costs were scaled to the size of the attached algae flow-way and include growth system and harvesting capital costs, as well as operational costs like electricity, labor, and maintenance. All costs were converted from their quoted year to 2018 dollars with the aid of cost indices [67]. CAPEX and OPEX estimates, along with the algae production determined the MBSP. Pretreatment costs were sourced from a water wash ash-reduction system [15], [38]. Capital costs of HTL and upgrading system were scaled from individual process equipment [41]. The operational costs considered included the costs associated with the consumption of electricity, natural gas, hydrogen, and the algae feedstock. The previously determined MBSP was used as the basis for the price of the feedstock. The MFSP was then calculated from the HTL system cost estimates. Detailed information for the attached algae flow-way and HTL system costs are found in Appendix A.

2.7. Sensitivity analysis

Two single point sensitivity analyses were conducted to identify variables that have the greatest impact on the biomass selling price and the renewable diesel selling price. Model inputs were varied ±20% from their baseline values. The resulting changes in the minimum biomass selling price (MBSP) and minimum fuel selling price (MFSP) were recorded.

2.8. Water quality trading

Water quality trading was utilized to evaluate the impact of this service on the system economics and place a value on the service of cleaning nutrient impaired waters with attached algae flow-ways. WQT is used to find the least cost solution by evaluating different nutrient reduction technologies. A variety of best management practices (BMP) exist to control emissions to water and they all vary in cost [68]. In this study, nitrogen and phosphorus credits are valued one-to-one [69]. A conservative estimate of \$4.5 kg-nutrient-removed^{-1} or \$4.5 per kg of total nitrogen (kg-TN^{-1}) and \$4.5 per kg of total phosphorus (kg-TP^{-1}) are used, which were the values previously leveraged by a pilot WQT program [69]. This is because the value of the WQT credits generated by the attached algae flow-ways are dependent on the design assumptions like the mass of nitrogen and phosphorus removed or the selling price of the biomass, which is dependent on the algae productivity. For example, at the Santa Monica Bay, CA subbasin, credit values for nutrient remediation ranged from \$5.8 kg-TN^{-1} to \$19 kg-TN^{-1} and from \$34 kg-TP^{-1} to \$110 kg-TP^{-1} depending on the algae productivity. Credit values for buyers are bound by the lowest cost solution and the abatement cost of the next highest alternative [70]. Previous work from Clippinger et al. (2021) leveraged wastewater treatment abatement costs (\$45 kg-TN^{-1} and \$45 kg-TP^{-1}) as the basis for their WQT credits [28]. In this view, a lower bound WQT credit value

of \$4.5 kg-nutrient-removed^{-1} and an upper bound of \$45 kg-nutrient-removed^{-1} are consistent with best practices and assumed in this study.

Chapter 3 – Results and discussion

3.1. Introduction

Environmental and economic results are first demonstrated at specific locations. The LCA modeling compares the environmental impacts of the renewable diesel to conventional diesel and other biodiesel pathways for a case study of Santa Monica Bay, CA. The TEA breaks down the price of the renewable diesel at three test locations (Santa Monica Bay, CA, Buffalo-San Jacinto, TX, and Sandusky, OH), and sensitivity analyses determined the high-impact variables. The feasibility of the proposed algal biorefining system was then explored by integrating geospatial data from 2,112 HUC8 subbasins to determine the price of the renewable diesel considering nutrient loadings in each watershed. Water quality trading was incorporated into the HUC8 analysis to place a value on the service of remediating dilute nutrients from the subbasins with attached algae flow-ways with two scenarios evaluated beyond the foundational work which does not include any monetary value for nutrient remediation.

3.2. Baseline life cycle analysis

The relative impacts for biofuel production in Santa Monica Bay, CA are broken down by major unit processes for each of the TRACI 2.1 life-cycle impacts and net energy ratio in Fig. 2. Each impact is compared to conventional diesel and soy-based biodiesel and discussed in more detail in the following sections. Tabular data of impacts are found in Appendix A.

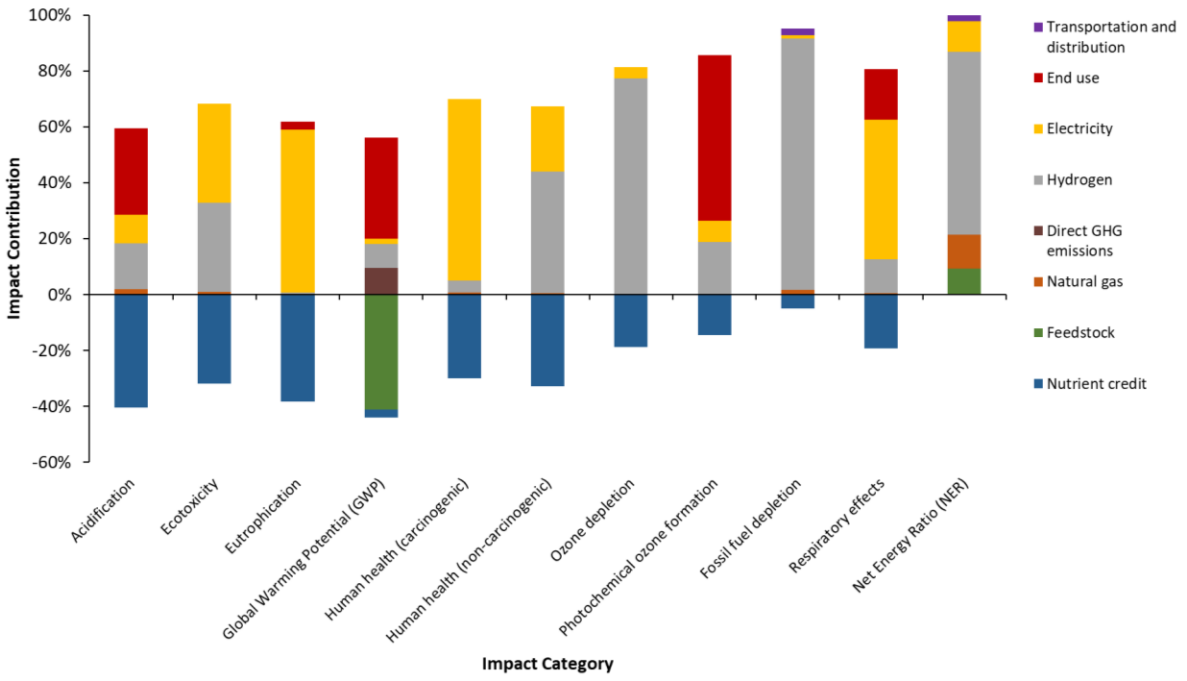

Fig. 2. TRACI 2.1 relative impacts for algal renewable diesel produced from algae from attached algae flow-ways in Santa Monica Bay, CA. Each impact category is broken down by major process variables. The light efficiency was set to 1.4%, corresponding to a local annual average productivity of 10.6 g m^{-2} day^{-1}.

3.2.1. Global warming potential (100-year horizon)

Global warming potential (GWP) is a measure of the radiative forcing from the release of greenhouse gases over a specified time horizon relative to CO_2 and is measured in carbon dioxide equivalents (CO_2 eq) [71]. A reduction in the GWP for biofuels, relative to the alternative, is required to be considered environmentally sustainable. The US renewable fuel standard (RFS) mandate for renewable diesel requires a 50% reduction in life cycle greenhouse gas emissions compared to conventional diesel [72]. On a WTW basis, the renewable diesel meets the RFS mandate with a GWP of 25 g CO_2 eq MJ^{-1}. The fuel end use contributed 75 g CO_2 eq MJ^{-1} [63], which counteracted -87 g CO_2 eq MJ^{-1} of carbon taken up by the feedstock. Other studies report GWPs between -37 and 377 g CO_2 eq MJ^{-1} [73] for HTL systems, but they all vary

in scope, scale, and system boundary. On a WTW basis, the baseline model GWP is similar those referenced.

3.2.2. Eutrophication

Eutrophication is the enrichment of nutrients in aquatic ecosystems that is accompanied by accumulation of algal biomass, including HABs, and is measured in nitrogen equivalents (N eq) [74]. Attached algae flow-ways are a tool for reducing nutrient concentrations in waterbodies which can ultimately reduce HABs. The eutrophication potential for the baseline model is 1.3×10^{-5} kg N eq MJ^{-1}. This represents a 68% reduction in eutrophication potential relative to conventional diesel. The eutrophication potential reported by Chen et al. (2021) (3.5×10^{-3} kg N eq MJ^{-1} [39]) for open raceway pond-cultivated and HTL converted algae biofuel is two orders of magnitude greater than the attached algae biofuel system because of the consumption of fertilizers in open raceway ponds. Unlike traditional (open raceway pond) algae cultivation methods, the attached algae flow-way requires no inputs of fertilizer to sustain growth. Rather, the nutrients are scrubbed from the water and are recovered from the biomass which displaces NH_3 and DAP fertilizers. The major contributor to the eutrophication potential is electricity use. The electricity consumption contributed to 94% of the N eq emissions. Thus reducing the pumping energy requirement or changing the grid mix to rely on electricity generation from sustainable sources would significantly reduce the eutrophication potential. The assumed 60% recovery of N and P from the biomass during conversion served as a nutrient displacement credit of 2.1×10^{-5} kg N eq MJ^{-1} in this study. If the magnitude of the nutrient credits outweighs the magnitude of end use and electricity consumption emissions, then this system can reverse the eutrophication potential associated with diesel consumption.

3.2.3. Net energy ratio

The net energy ratio (NER) is the overall energetic effectiveness of a system [75]. The NER for this system is 0.33 MJ MJ^{-1}, indicating that more energy is contained in the biofuels than is required for production. Values less than one are favorable, but the goal is to have a NER lower than conventional diesel, 0.19 [63,64]. For reference, soy-based biodiesel has a NER of 1.64 [76]. The NER of other HTL systems range from 0.30 to 1.24 [39,75,77], but these variations are largely due to differences in HTL plant layout and conversion yields. This system is based on the work done by Chen et al. (2021) and therefore does not include a co-located hydrogen generation plant for the biofuel upgrading but rather the purchasing of hydrogen. Hydrogen is the greatest contributor to the NER for this system since it is treated as an operating cost. Jones et al. (2014) included a hydrogen plant in their HTL system, lowering their NER to 0.22 [41]. Incorporating a hydrogen plant to this system may allow the NER for this system to achieve parity with conventional diesel but could negatively impact other sustainability metrics.

3.2.4. Acidification

Acidification is a measure of how a system increases the concentration of hydrogen ions or components that increase the acidity within local environments like NH_3 or DAP and is measured in sulfur dioxide equivalents (SO_{2e} eq). Acidification damages human-built structures, water bodies, plants, and animals [74]. The acidification potential for the baseline model (1.5×10^{-5} kg SO_2 eq MJ^{-1}) is nearly an order of magnitude lower than conventional diesel and soy biodiesel (1.4×10^{-4} and 1.2×10^{-4}, respectively). Fuel end use emissions are the largest contributor (52%) to this metric, but the nutrient credits in the algal turf system reduce the net acidification potential for the system. It should also be considered that field trials from the Sandia Testbed indicate that the flow-ways raise the pH of the treated water by removing

dissolved carbon, which may also contribute to a further reduction in the acidification potential for the system. For example if a pH change from 7 to 8 is observed in the source waters from an attached algae flow-way, a reduction in SO_2 eq emissions ($-2.38*10^7$ kg SO_2 eq hr^{-1}) results in a reduction in the acidification potential for the system (-102 kg SO_2 eq MJ^{-1}). This reduction causes the acidification potential for the system to turn negative, meaning the attached algae flow-ways can reverse the acidification potential associated with diesel consumption. Sample calculations are found in Appendix A.

3.2.5. Ecotoxicity

Ecotoxicity represents the susceptibility of freshwater ecosystems to chronic toxins emitted from human activities and is measured in comparative toxic units for ecotoxicity (CTUe) [78]. The baseline model results in an ecotoxicity of 3.5×10^{-2}CTUe MJ^{-1}which is 1.8x greater than conventional diesel, but a factor of 2.0x less than soy biodiesel. Electricity and hydrogen consumption are drivers of CTUe emissions for this system (52% and 47%, respectively), whereas the nutrient credits are the source of CTUe reductions. Inclusion of a hydrogen plant in the process model and sourcing electricity from sustainable sources offer the greatest opportunities reduce the ecotoxicity.

3.2.6. Human health (carcinogenic and non-carcinogenic)

Carcinogenic and non-carcinogenic human health impacts from 3000 substances are assessed with the TRACI 2.1 assessment method and are measured in comparative toxic units for humans (CTUh) [74]. The human health impacts of the algal renewable diesel for the carcinogenic and non-carcinogenic categories are 2.5×10^{-10} CTUh MJ^{-1} and 1.6×10^{-9} CTUh MJ^{-1}, respectively. The carcinogenic impact for algal renewable diesel is less than conventional diesel by a factor of 1.5x and less than soy biodiesel by a factor of 3.0x. Electricity consumption

dominates carcinogenic emissions (93%) for the algal renewable diesel. The non-carcinogenic impact for algal renewable diesel is greater than conventional diesel by a factor of 2.1x, but less than soy biodiesel by a factor of 1.8x. Hydrogen consumption constitutes most of the non-carcinogenic emissions (65%) for the algal renewable diesel.

3.2.7. Ozone depletion

Stratospheric ozone reflects harmful UV radiation away from earth. The ozone depletion potential tracks the relative contribution of substances that degrade of the ozone layer and is measured in Trichlorofluoromethane equivalents (CFC-11 eq) [74]. The ozone depletion potential for the baseline model is 3.7×10^{-9} kg CFC-11 eq MJ^{-1}. The impact from conventional diesel is greater than the impact from the algal renewable diesel by a factor of 5.4x. Soy biodiesel exhibits a lesser ozone depletion potential than algal renewable diesel by a factor of 1.3x. Hydrogen consumption drives most of the ozone depletion emissions (95%) for the algal renewable diesel.

3.2.8. Photochemical ozone formation

Smog, primarily originating from vehicle tailpipes and electric power utilities, reacts with sunlight to produce ozone [79]. Ground level ozone is harmful to human health and can lead to respiratory issues and damage various ecosystems and is measured in ozone equivalents (O_3 eq) [74]. In the photochemical ozone formation category, the baseline model releases 1.2×10^{-3} kg O_3 eq MJ^{-1}. The impact for algal diesel is less than conventional diesel by a factor of 1.7x and less than soy biodiesel by a factor of 2.2x. The end use of the algal renewable diesel is the largest contributor for this impact (69%). The differences between these systems can be explained by a reduction in emissions associated with electricity and natural gas consumption for the flow-ways (i.e. less energy intensive), as well as the nutrient credits the flow-ways receive.

3.2.9. Fossil fuel depletion

Fossil fuel depletion accounts for the depletion fossil fuels, which are a non-renewable resource. The baseline model has an impact of 2.8×10^{-1} MJ-surplus MJ^{-1} in the fossil fuel depletion category, which is greater than conventional diesel by a factor of 1.6x and greater than soy biodiesel by a factor of 11x. Hydrogen consumption for the algal renewable diesel is the primary driver for this impact category (97%). This result is consistent with expectations since fossil fuels generally require less processing than algae biofuels. Energy and resources like hydrogen are required throughout the entire lifecycle—from algae cultivation through fuel conversion and upgrading—whereas crude oil does not have a cultivation or conversion processes. Soy biodiesel does not consume hydrogen during processing and is better than algal renewable diesel in terms of fossil fuel depletion.

3.2.10. Respiratory effects

Particulate matter found in the air can lead to respiratory illnesses. Particulate matter emissions originate from combustion of fuels and through chemical reactions in the air [74]. Respiratory effects is defined as emissions of particulates that are 2.5 microns or less in diameter is measured in particulate matter 2.5 equivalents (PM2.5 eq) [80]. The baseline model has an impact of 1.5×10^{-5} kg PM2.5 eq MJ^{-1} in the respiratory effects category. The impact from algal renewable diesel is less than the impact from conventional diesel by a factor of 1.1x and less than soy biodiesel by a factor of 1.5x. Electricity consumption contributes the most to this impact category (62%) for the algal renewable diesel. This result demonstrates that emissions that occur upstream are just as important as the emissions out of the tailpipe. A clean grid mix is crucial to reducing particulate matter emissions.

3.2.11. Life cycle analysis interpretation

All the TRACI impacts are important to consider when evaluating a technologies effect on the environment, but GWP, eutrophication, and NER are most relevant for this biofuel system. The renewable diesel meets the RFS mandate by achieving a 71% reduction in lifecycle CO_{2eq} emissions relative to conventional diesel. The nutrients credits allow this system to reduce the eutrophication potential associated with fossil fuel consumption, but the burden of the fertilizer is carried by the end-user and how the fertilizer is used is out of the scope of this study. The end-fate of the fertilizer may be back in the watersheds they are recovered from, but now the nutrients are recycled in the system, rather than being consumed from chemical fertilizers that commonly originate from crude oil extraction and refining. This system also demonstrated a NER less than one, but advancements are required to approach the NER for conventional diesel. Looking across most impact categories, the results are largely influenced by emissions associated with the consumption of hydrogen for fuel upgrading and electricity in the growth phase and fuel end use. While end use emissions are unlikely to decrease, it is possible to reduce the lifecycle emissions by generating hydrogen onsite rather than bearing the burdens of transporting it from conventional, emissions-intensive sources [66]. However, the tradeoff between diverting off-gases from supplemental heating to an on-site hydrogen plant need to be investigated since additional natural gas would then be required to raise the feedstock to the reactor temperature. Reductions are also possible by sourcing electricity from sustainable sources like wind or solar rather than fossil fuels, but this again has complications associated with consistent energy supply. The results demonstrate that the baseline model produces renewable diesel that is an environmentally sustainable alternative to conventional diesel.

The results from this study highlight the consequences that design decisions have on the impacts discussed. Minimizing uncertainties in results allows for more confidence in making decisions, but assumptions and simplifications are often impossible to avoid. For this system, more work is needed to understand the extent to which bioavailable nitrogen and phosphorus are recovered from the conversion of the biomass [81]. The recovery rate directly impacts the nutrient credits and counters harmful emissions across most impact categories. For example, if the nutrient recovery rate is set to 80%, then life cycle GHG emission reduces by 8% while net eutrophication potential reduces by 54%. Proportional changes in the opposite direction are observed when the nutrient recovery rate is set to 40%. This shows that more research is needed to validate the assumption proposed by Chen at al. (2021) and Jones et al (2014) [39], [41]. Other uncertainties in the system exist, but nutrient recovery is most significant because of its impact on the LCA.

3.3. Baseline techno-economic assessment

The baseline TEA was applied to three HUC8 subbasins: Santa Monica Bay, CA; Buffalo-San Jacinto, TX; and Sandusky, OH. The Santa Monica Bay, CA location has the highest concentration of TN and TP, 21.9 mg-TN L^{-1} and 3.90 mg-TP L^{-1} and is nitrogen limiting with an inflow TN:TP ratio of 12.4 mol mol^{-1}. Even though Santa Monica Bay, CA had a lower flow rate of water through the subbasin 20.7 m^3 s^{-1} (472 MGD), high TN and TP concentrations led to greater TN and TP loadings (kg day^{-1}) than the other two locations. Both Buffalo-San Jacinto, TX and Sandusky, OH had similar TN concentrations (6.51 and 6.01 mg-TN L^{-1}, respectively), but Buffalo-San Jacinto's TP concentration (0.812 mg-TP L^{-1}) is greater than Sandusky's (0.300 mg-TP L^{-1}). Buffalo-San Jacinto, TX and Sandusky, OH are both phosphorus limited with inflow TN:TP ratios of 17.7 mol mol^{-1} and 44.2 mol mol^{-1}, respectively. The flow

rate of water through the subbasins are 69.4 $m^3 s^{-1}$ (1584 MGD) for Buffalo-San Jacinto, TX and 61.4 $m^3 s^{-1}$ (1401 MGD) for Sandusky, OH. These nutrient loadings, along with productivity estimates from the algae growth model fed into the attached algae flow-way process model, where the systems were sized to treat the incoming water with outputs used to evaluate the economic viability at each location.

Three different growth rates were modeled to account for the varying degrees of technological readiness for the attached algae flow-ways. For the lowest US maximum annual productivity tested (12.4 g m^{-2} day^{-1}), Santa Monica Bay, CA, Buffalo-San Jacinto, TX, and Sandusky, OH had local annual average productivities of 10.6 g m^{-2} day^{-1}, 8.77 g m^{-2} day^{-1} and 7.56 g m^{-2} day^{-1}, respectively. This resulted in attached algae flow-way module areas and algae productions of: 33.3 km^2 and 352 tonne day^{-1} for Santa Monica Bay, CA; 28.5 km^2 and 250 tonne day^{-1} for Buffalo-San Jacinto, TX; and 11.6 km^2 and 89.0 tonne day^{-1} for Sandusky, OH. The effect of increasing the algae productivity reduced the area required for treatment but kept the algae production constant. Increasing the US maximum annual productivity from 12.4 g m^{-2} day^{-1}, to 25 g m^{-2} day^{-1} and 40 g m^{-2} day^{-1} decreased attached algae flow-way module areas at each location by a factor 2.02x and 3.23x, respectively. The attached algae flow-way module areas and algae production values were then used to determine the minimum biomass selling prices.

For the baseline TEA model, the MBSP ranged from \$269 $tonne^{-1}$ to \$1,447 $tonne^{-1}$ across the three locations. Santa Monica Bay, CA exhibited the lowest biomass prices for every productivity evaluated (\$858 $tonne^{-1}$, \$427 $tonne^{-1}$, and \$269 $tonne^{-1}$ for 12.4 g m^{-2} day^{-1}, 25 g m^{-2} day^{-1}, and 40 g m^{-2} day^{-1}, respectively). The MBSP at Buffalo-San Jacinto ranged from \$331 $tonne^{-1}$ to \$1,046 $tonne^{-1}$, while the MBSP at Sandusky ranged from \$470 $tonne^{-1}$ to \$1,447

tonne^{-1}. The biomass prices are driven by attached algae flow-way module costs, which represent 86% of the CAPEX and roughly 50% of the total MBSP. Despite Santa Monica Bay, CA requiring the largest area for remediating the water (increased module costs), the algae production was high enough to reduce the MBSP to levels lower than both Buffalo-San Jacinto and Sandusky. This is because Santa Monica Bay, CA had greater TN and TP loadings and greater algae productivities, which translates to more algae production. The biomass prices informed the biorefinery economic model where the price of the renewable diesel was determined.

The MFSP at each location for all three productivities is broken down by sub-process in Fig. 3. The price of the renewable diesel ranged from $1.20 per cubic decimeter (dm^{-1}) to $5.10 dm^{-1} or $4.56 per gallon of gasoline equivalent (GGE^{-1}) to $19.3 GGE^{-1}, with Santa Monica Bay, CA having the lowest MFSP for each productivity. Feedstock prices dominated system economics for every scenario and contributed from 56% to 86% of the total price of the renewable diesel selling price. Indirect costs and HTL costs made up 71% of the CAPEX costs on average. Of the remaining OPEX costs, fixed costs (labor, maintenance, and insurance) are the next major contributor. Fixed costs ranged from 4.3% to 18% of the price of the renewable diesel. Like the LCA, 60% of the nitrogen and phosphorus in the algae is recovered and sold as a fertilizer co-product. The fertilizer co-product revenues did not greatly alter the MFSP and the impact on reducing the renewable diesel price ranged from $0.095 dm^{-1} ($0.36 GGE^{-1}) to $0.19 dm^{-3} ($0.71 GGE^{-1}).

Any reductions to the MFSP are mainly due to reductions in the feedstock price. As previously discussed, Santa Monica Bay, CA had high nutrient loadings and productivities relative to the other locations. These conditions allowed for a high level of algae production

(economies of scale) which offset the production costs and lowered the MBSP. Future work is needed to optimize algae productivities to maximize algal biomass production. Renewable diesel will be competitive with conventional diesel if the feedstock price is minimized in the proposed system.

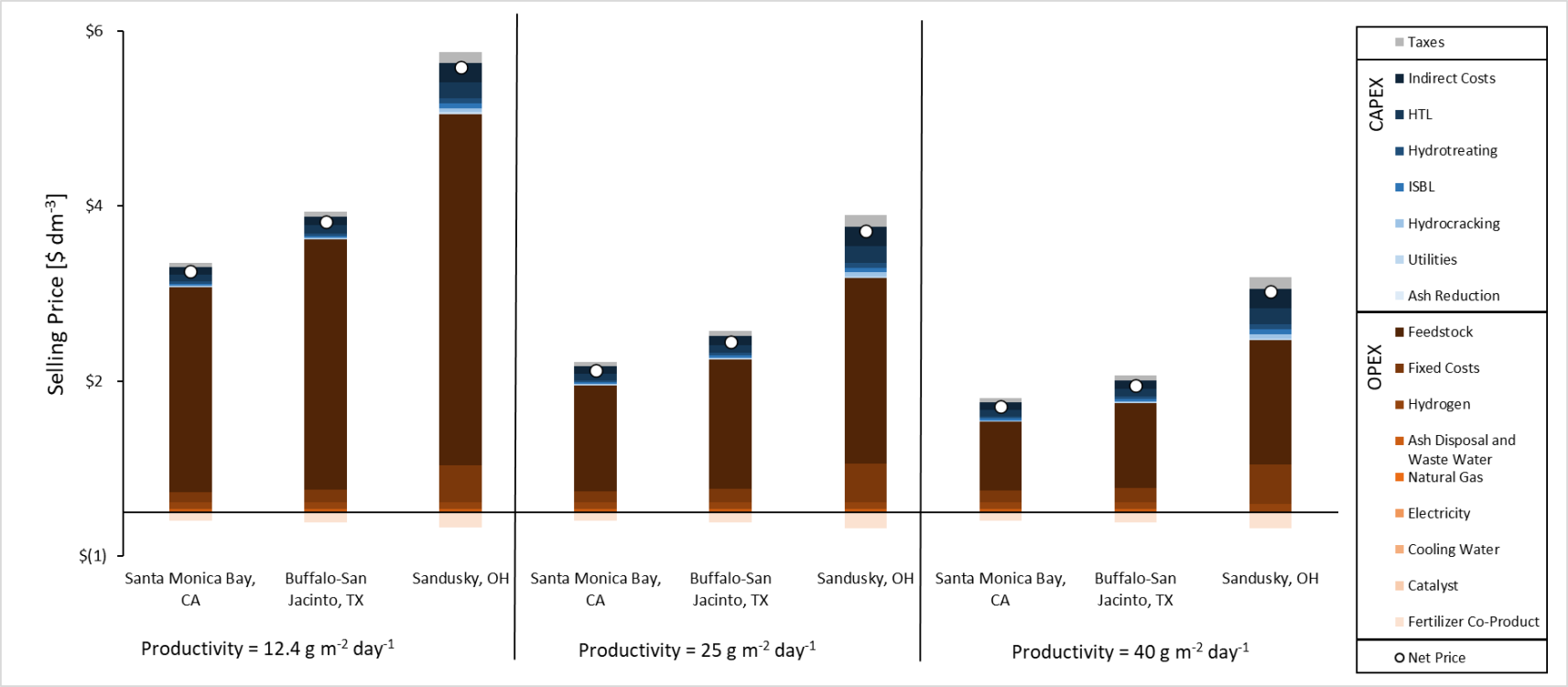

Fig. 3. Renewable diesel minimum fuel selling price for three target locations broken down by capital expense (CAPEX) and operational expenses (OPEX) contributions. Three algae productivities were tested for each location (12.4, 25, and 40 g m-2 day-1). OPEX costs are shown in shades of blue and CAPEX costs are shown in shades of maroon. The net prices are indicated with a white point.

3.4. Baseline sensitivity analysis

Single point sensitivity analyses were conducted on the TEA at Santa Monica Bay, CA. Major input variables were perturbed ±20% from their baseline values. The resulting price changes are seen on the tornado plots in **Error! Reference source not found.**Fig. 4. The US maximum annual productivity was set to 12.4 g m^{-2} day^{-1} for this analysis, translating to a local annual average productivity of 10.6 g m^{-2} day^{-1}.

The algae productivity is one of the most impactful variables on the MBSP as expected. Decreasing the productivity by 20% decreased the biomass price by 17% from its baseline value of \$946 ton^{-1}. This is due to an equivalent 20% increase in the attached algae flow-way module area required to remediate the water. For a given algae production (kg day^{-1}), increased module areas increase the capital costs, which are the largest contributor (Figure 3) which increases the MBSP. Similarly, when the productivity increases, the required area decreases, reducing the biomass price. This demonstrates that productivities are the crux of this system, further validating previous conclusions drawn by Cruce et al. (2021) [73]. This process model addresses some of the uncertainties by using a geographically resolved algae growth model rather than assuming the same productivity at every test site.

Operational days is the number of days a test site is operational per year and accounts for the number of freezing days. The operational days does not affect daily or hourly flows, instead it affects the total consumption of raw materials and production of products over the course of a year. Increasing and decreasing the operational days resulted in biomass price changes that are similar in magnitude to productivity changes. The high degree of model sensitivity to operational days shows that more work is needed to address the limitations of a 1st order growth model.

The inflow TN and TP concentrations, as well as the target effluent TN and TP concentrations had little effect on the MBSP. Santa Monica Bay's TN and TP concentrations are much higher than the specified effluent limits. Thus, changing these parameters only slightly reduced the amount of TN and TP that could be removed with an attached algae flow-way. Had the inflow concentrations been closer to the effluent concentrations, greater sensitivity in the MBSP to these changes would be observed.

For the MFSP, ash content is one of the least impactful variables. Unlike in previous studies, this model assumes a lower initial ash content of 20wt% based on new data from Sandia National Laboratories. Increasing ash content by 20% raised the MFSP to \$2.77 dm^{-3} (\$10.5 GGE^{-1}). If the ash content was set higher to 60wt%, then the MFSP would increase to \$3.01 dm^{-3} (\$11.4 GGE^{-1}). The increase is primarily attributed to the HTL system as additional ash increases the amount of water in the system and thus the size of the HTL system. Higher ash contents additionally result in higher operational costs associated with natural gas and electricity consumption due to the added parasitic load in conversion of excess water. Reductions in ash content may be achieved through implementation of more upstream ash reduction technologies or operational changes that result in lower ash contents during cultivation or in harvested biomass.

Biocrude yields are also important to system economics. Increasing the biocrude yield to 54% decreased the MFSP of the renewable diesel by 16%. Decreasing the yield to 36% demonstrated a greater impact by increasing the MFSP by 24%. Studies have reported biocrude yields between 35% to 60% with reactor temperatures, reaction times, and solid loadings pointed to as the key drivers [39], [41], [40], [82–88]. It is possible to improve biocrude yields by boosting protein and lipid content in the algae biomass, however high protein content is

associated with increased nitrogen content, lowering the quality of the resulting fuel [32], [89]. More research is needed to optimize reaction dynamics and algae compositions. For example, seeding the flow ways with algae that contain high lipid fractions could improve fuel yields due to changes in composition.

Another impactful variable to the MFSP is the biomass price, as discussed in section **Error! Reference source not found.**, the feedstock price contributes to most of the renewable d iesel costs, with the attached algae flow-way module costs contributing nearly 50%. Attached algae flow-ways are not operationally intensive processes [32], so the most gains will be made by addressing the capital costs. Although it is possible to reduce the module costs by increasing algal productivities, the limits of biology can only be pushed so far; photosynthetic efficiencies for representative algae species are estimated to be significantly higher than terrestrial plants, but photosynthetic efficiencies greater than 5% have not been observed for outdoor algae production [90]. If productivities are maximized, then only other viable option to reduce the biomass price is by valuing the service the algae provide for remediating contaminated water.

A)

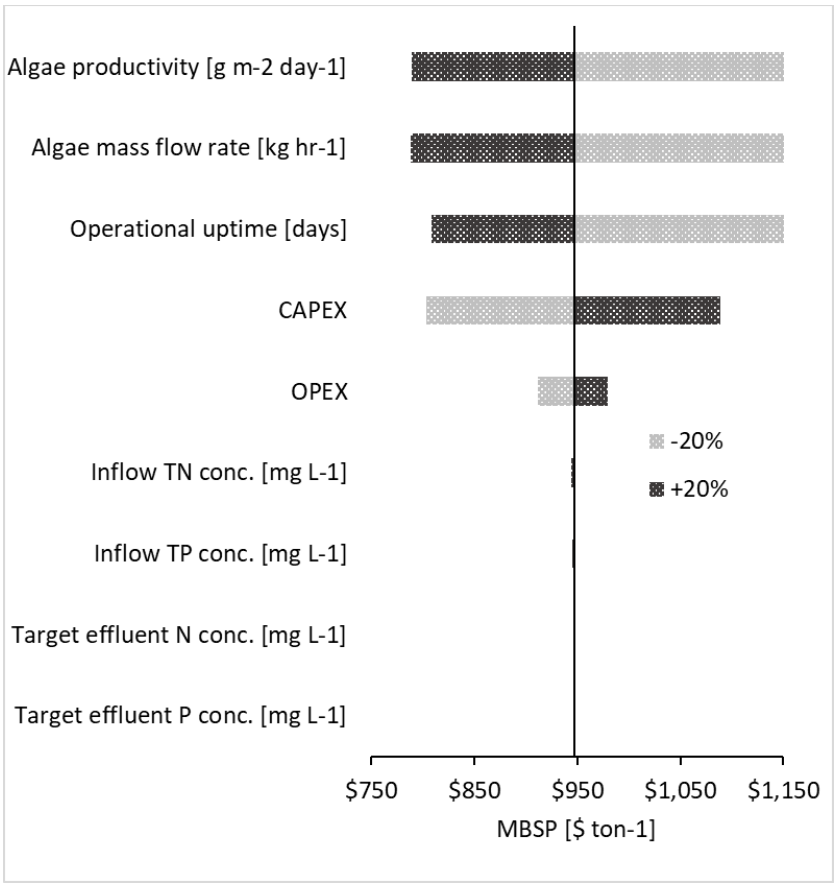
Algae productivity [g m-2 day-1]
Algae mass flow rate [kg hr-1]
Operational uptime [days]
CAPEX
OPEX
Inflow TN conc. [mg L-1]
Inflow TP conc. [mg L-1]
Target effluent N conc. [mg L-1]
Target effluent P conc. [mg L-1]
-20%
+20%
$750
$850
$950
$1,050
$1,150
MBSP [$ ton-1]

B)

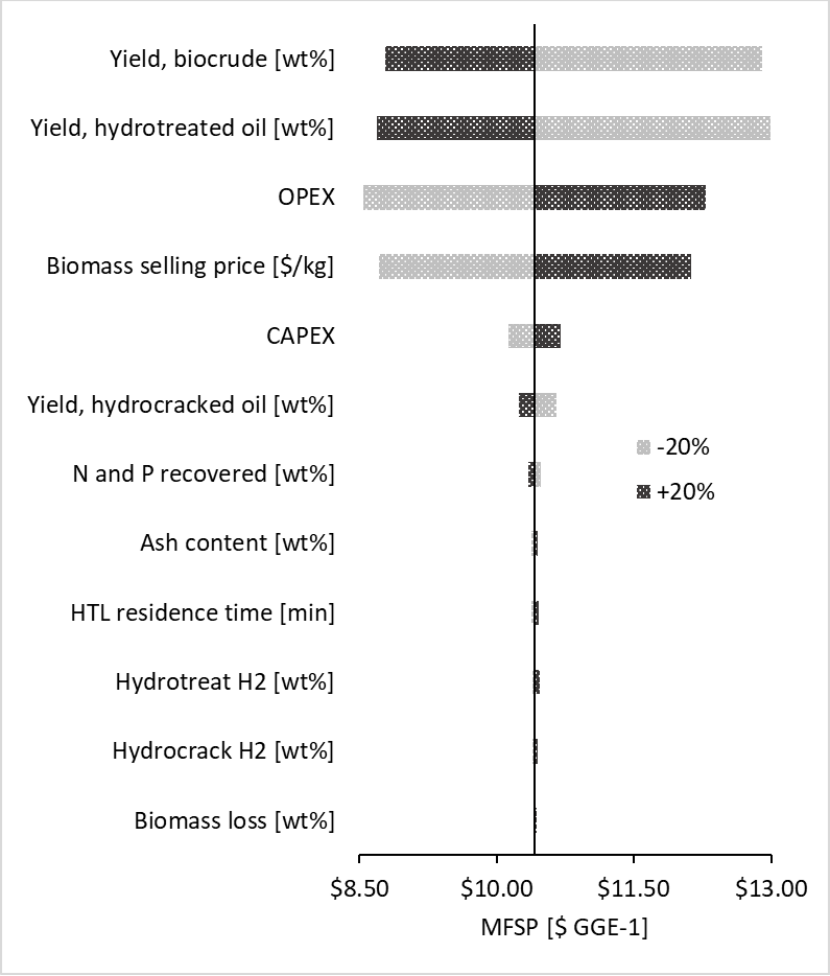

Fig. 4. Tornado plots of (a) minimum biomass selling price (MBSP) sensitivity to changes in major input variables and (b) minimum fuel selling price (MFSP) sensitivity to changes in major input variables. All major input variables were perturbed +/- 20% from their baseline values. The resulting changes in prices are plotted

3.5. HUC8 model results

The baseline process model was applied to each HUC8 subbasins in the contiguous US with the three light efficiencies (1.4%, 2.8% and 4.5%), translating to three US maximum annual productivities (12.4 g m^{-2} day^{-1}, 25 g m^{-2} day^{-1}, 40 g m^{-2} day^{-1}, respectively). Following the same methodology as the baseline locations, attached algae flow-ways were sized to treat the delivered loads of nitrogen and phosphorus from all 2,112 HUC8 subbasins. The resulting biomass production and prices informed the biorefinery process models to produce renewable diesel and

determine the MFSP. The service of cleaning watersheds with attached algae flow-ways was valued by the inclusion of WQT credits. The following sections contain the results for MFSP of the renewable diesel and the effects of incorporating WQT credits on the fuel price.

3.5.1. HUC8 model techno-economic assessment

Maps displaying the renewable diesel MFSP at all HUC8 subbasins for the three biomass productivities evaluated are shown in Fig. 5**Error! Reference source not found.**Some subbasins already meet the specified effluent limits and do not require any treatment with these locations defined as NA and show up as a grey color on the maps. Many other locations are on the cusp of meeting the TN and TP limits and their resulting MFSPs are so large a price cutoff criterion is introduced for clarity on the maps. These locations generally exhibited low nutrient loadings which led to low algae production and high fuel prices. Locations with prices greater than \$6.61 dm^{-3} (\$25 GGE^{-1}) are indicated with an orange color on the maps. A consistent green color scale is used across the maps for prices between \$0 dm^{-3} to \$6.61 dm^{-3} (\$0 GGE^{-1} to 25 GGE^{-1}) to clearly illustrate the change in prices from changes in productivities.

Productivities impact the feasibility of the system. Assuming a US maximum annual productivity of 12.4 g m^{-2} day^{-1} resulted in the lowest MFSP of \$2.75 dm^{-3} (\$10.4 GGE^{-1}) and an average price of \$5.23 dm^{-3} (\$19.8 GGE^{-1}) for prices below \$6.61 dm^{-3} (\$25 GGE^{-1}). There are 123 locations with prices below this average and only 6 locations with a price less than \$3.95 dm^{-3} (\$15 GGE^{-1}). Increasing the US maximum annual productivity to 25 g m^{-2} day^{-1} decreased both the lowest MFSP to \$1.62 dm^{-3} (\$6.14 GGE^{-1}) and the average price to \$3.79 dm^{-3} (\$14.4 GGE^{-1}) for prices below \$6.61 dm^{-3} (\$25 GGE^{-1}). There are 202 locations with a price below the average and 24 locations with a price below \$2.64 gm^{-3} (\$10 GGE^{-1}). Increasing the US maximum annual productivity to 40 g m^{-2} day^{-1} reduced the lowest MFSP to \$1.21 dm^{-3} (\$4.56

GGE^{-1}) and an average price of \$3.78 dm^{-3} (\$14.3 GGE^{-1}) for prices below \$6.61 dm^{-3} (\$25 GGE^{-1}). The number of locations with a price below the average increased to 227, providing 9 locations with a price below \$2.64 gm^{-3} (\$10 GGE^{-1}). The concentration of locations with favorable MFSPs remained relatively consistent across corn belt for the three US maximum annual productivities tested, but in general, increasing the US maximum annual productivity decreases the renewable diesel MFSP.

The subbasins varied in initial conditions, but there are several key features that lead to lower MFSPs. As indicated by the darker green color on the maps, the highest concentration of favorable locations is found in the Midwest. Also known as the corn belt, the Midwest is responsible for over a third of the world's corn and soybeans [91]. These agricultural products require large quantities of chemical fertilizer. As a result, subbasins located within the Midwest suffer from high nitrogen and phosphorus loadings because the fertilizers leach off the arable land. Increased loadings of nitrogen and phosphorus result in more algae production because more nutrients are available for the microorganisms to thrive. Maps showing the TN and TP concentrations of the HUC8 subbasins are found in Appendix A. As the production of algae increases, facilities reach the economies of scale required to see a decrease in the renewable diesel selling price.

Operational days is another indicator of a favorable renewable diesel price. Temperature effects on algae growth were approximated with operational days to differentiate regions that are susceptible to harsh winters from regions that can maintain year-round algae production. Decreasing operational days results in idle capital because a given location is sized to treat a specified load of TN and TP but cannot operate the entire year, causing the algae production to decrease and the MFSP to increase. Southern states like Texas, Louisiana and Florida did not

suffer from deep freezes and had plant capacities of 365 days per year. The number of freezing days increases as attached algae flow-ways are deployed further north. For example, subbasins located near Glacier National Park produce algae for roughly 220 days a year. These northern locations demonstrated some of the highest MFSPs. A map of the operational days for every HUC8 subbasin is found in Appendix A.

Unsurprisingly, high productivities correlate with lower MFSPs. The desert southwest receives the most sunlight compared to other states. It is expected that locations near the desert southwest would have the highest productivities, while northeastern states like Vermont and New Hampshire would have the lowest productivities. Regions with lower productivities require larger areas for treating the same amount of TN and TP when compared to regions with higher productivities. Larger attached algae flow-way module areas increase the capital costs associated with the biomass, which increases the price of the renewable diesel. Productivity maps are also found in Appendix A.

While none of these variables alone can predict the economic feasibility of individual subbasins, when combined, they point to the optimum conditions for this system: high nutrient loadings, high productivities, and maximal annual operational days. It is possible to improve operating conditions for the attached algae flow-ways like algae productivities, but increasing productivities offers diminishing returns for reducing the renewable diesel MFSP. If renewable diesel is to be competitive with conventional diesel, it is imperative that the service the algae provides for removing nitrogen and phosphorus from water is valued. Water quality trading credits offer a solution for valuing this service and can dramatically improve the system economics.

A)

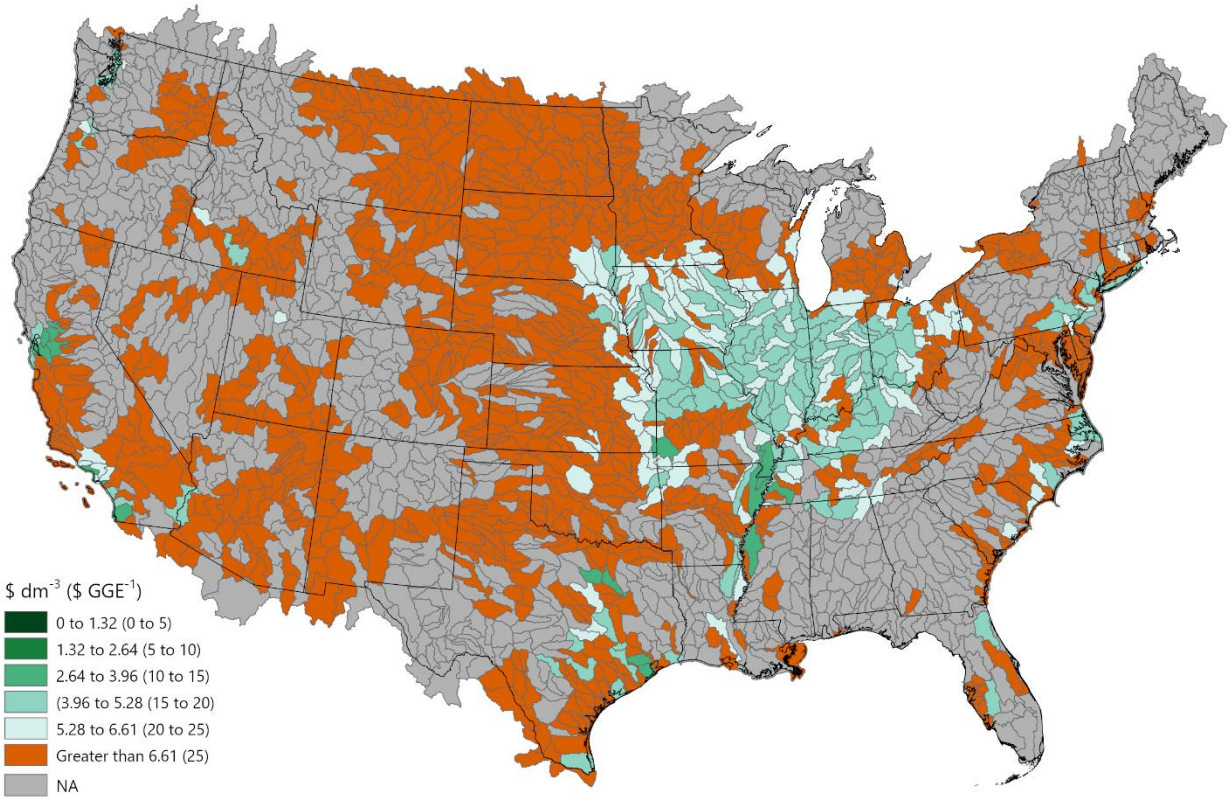
$ dm-3 ($ GGE-1)
0 to 1.32 (0 to 5)
1.32 to 2.64 (5 to 10)
2.64 to 3.96 (10 to 15)
(3.96 to 5.28 (15 to 20)
5.28 to 6.61 (20 to 25)
Greater than 6.61 (25)
NA

B)

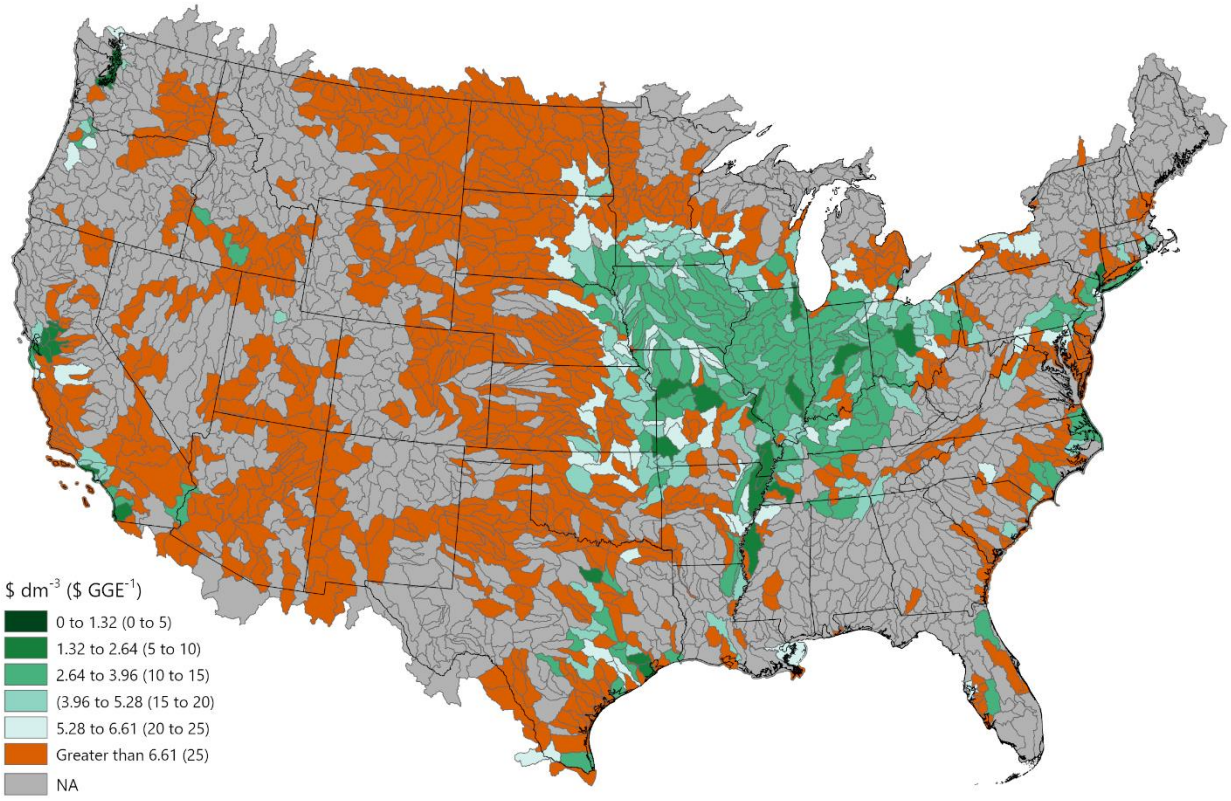
$ dm-3 ($ GGE-1)
0 to 1.32 (0 to 5)
1.32 to 2.64 (5 to 10)
2.64 to 3.96 (10 to 15)
(3.96 to 5.28 (15 to 20)
5.28 to 6.61 (20 to 25)
Greater than 6.61 (25)
NA

C)

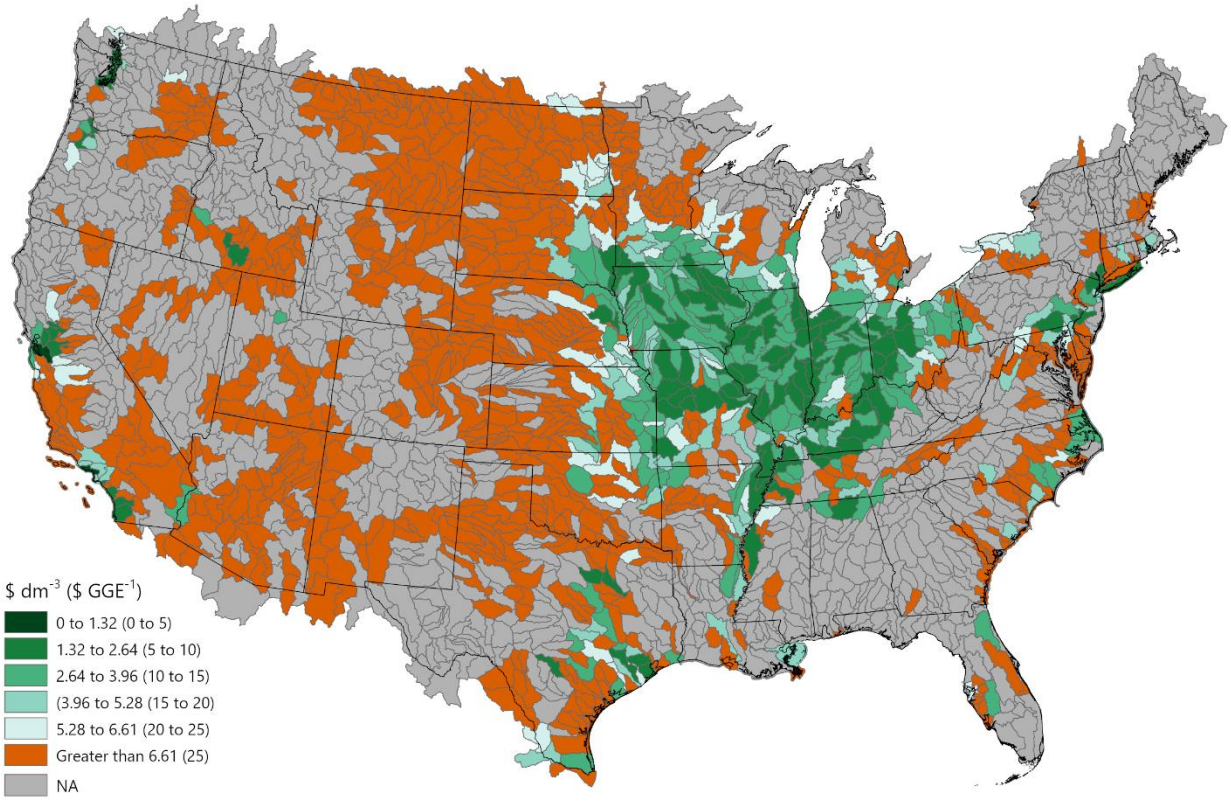
$ dm-3 ($ GGE-1)
0 to 1.32 (0 to 5)
1.32 to 2.64 (5 to 10)
2.64 to 3.96 (10 to 15)
(3.96 to 5.28 (15 to 20)
5.28 to 6.61 (20 to 25)
Greater than 6.61 (25)
NA

Fig. 5. Maps showing the MFSP for renewable diesel at the HUC8 level for maximum productivities of (a) 12.4 g m^{-2} day^{-1}, (b) 25g m^{-2} day^{-1}, and (c) 40 g m^{-2} day^{-1}.

3.5.2. HUC8 model water quality trading

Water quality trading is a market-based approach to finding the least cost solution for cleaning watersheds [64]. A WQT credit is generated when a pollutant, like nitrogen or phosphorus, is removed from surface waters. Polluters facing high control costs can meet their regulatory obligations by offsetting their emissions through the purchase of WQT credits. Water quality improves and the buyer can reduce their emissions at a lower cost. Two different water quality trading credit scenarios were added into the economic model and their effects on the MFSPs are shown in Fig. 6. A productivity of 25 g m^{-2} day^{-1} was assumed because it represents a feasible productivity for the attached algae flow-ways to achieve in the near-term and does not overstate the effects of higher productivities on the MFSP. Two levels of WQT credits, \$4.5 kg-nutrient-removed^{-1} (\$10 lb-nutrient-removed^{-1}) and \$45 kg-nutrient-removed^{-1} (\$100 lb-nutrient-removed^{-1}), were selected to represent the bounds of the possible value of the credits this system would receive [28,69]. The WQT credits represent an additional revenue stream for the total mass of nitrogen and phosphorus removed by the attached algae flow-ways over an operational year.

When a credit value of \$4.5 kg^{-1} is included in the analysis, the lowest MFSP drops to \$1.01 dm^{-3} (\$3.84 GGE^{-1}) in Santa Monica Bay, CA. This modest WQT credit results in a renewable diesel price that is on par with the price of conventional diesel. The average price of the renewable diesel for prices lower than \$6.61 dm^{-3} (\$25 GGE^{-1}) also dropped to \$3.59 dm^{-3} (\$13.6 GGE^{-1}) when compared to the same productivity with no WQT credits. The concentration of favorable locations also expanded to include more regions in western states like Idaho and Utah, with 225 locations with a MFSP below the average. However, the term ‘favorable’ is

relative to the entirety of the contiguous US; a price target of \$1.32 dm^{-3} (\$5 GGE^{-1}) is more representative of a viable location. There are only three locations in the US with MFSPs below \$1.32 dm^{-3} (\$5 GGE^{-1}) under this water trading credit scenario. Given that there are few locations that achieve price parity with petroleum fuels, higher WQT credit values are necessary to see further reductions in the renewable diesel MFSP from the proposed algae system.

Leveraging WQT credits valued at \$45 kg-nutrient-removed^{-1} (\$100 lb-nutrient-removed^{-1}) creates a new classification of favorable locations. As seen in Figure 6, there are now locations with prices below \$0 dm^{-3} (\$0 GGE^{-1}) and are denoted with shades of purple. When the price of the renewable diesel turns negative, the value of the fuel becomes negligible as the value of the service that the algae provide for removing dilute nutrients covers all costs of the system. This means that the fuels are no longer required to make the biorefinery profitable. The greater the WQT credit value, the more negative the MFSP and the more revenue investors can make in each subbasin. There are now 398 locations where the price of renewable diesel is less than \$0 dm^{-3} (\$0 GGE^{-1}), with the lowest MFSP of \$-9.97 dm^{-3} (\$-37.7 GGE^{-1}).

These results highlight the impact the algal system can have in dilute nutrient remediation where traditional wastewater treatment systems cannot compete. Traditional wastewater systems cost approximately \$45 kg-nutrient-removed^{-1} (\$100 lb-nutrient-removed^{-1}) to remediate surface waters due to the large volumes of water that must be processed. The results also demonstrate that traditional locations considered for algal systems—the gulf coast or the desert southwest—are not optimal as these watersheds are not contaminated with high nutrient loads. However, for the locations identified as the best deployment zones for an attached algae flow-way, there may be challenges in terms of land availability. Land in the Santa Monica Bay, CA subbasin is scarce and deploying a large attached algae flow-way is likely unattainable. Less populated regions

downstream of major polluters along the Colorado River or the Mississippi River are potential deployment locations. As WQT values reach \$45 kg-nutrient removed^{-1} (\$100 lb-nutrient-removed^{-1}) land availability is expected to be the limiting factor in some locations.

A)

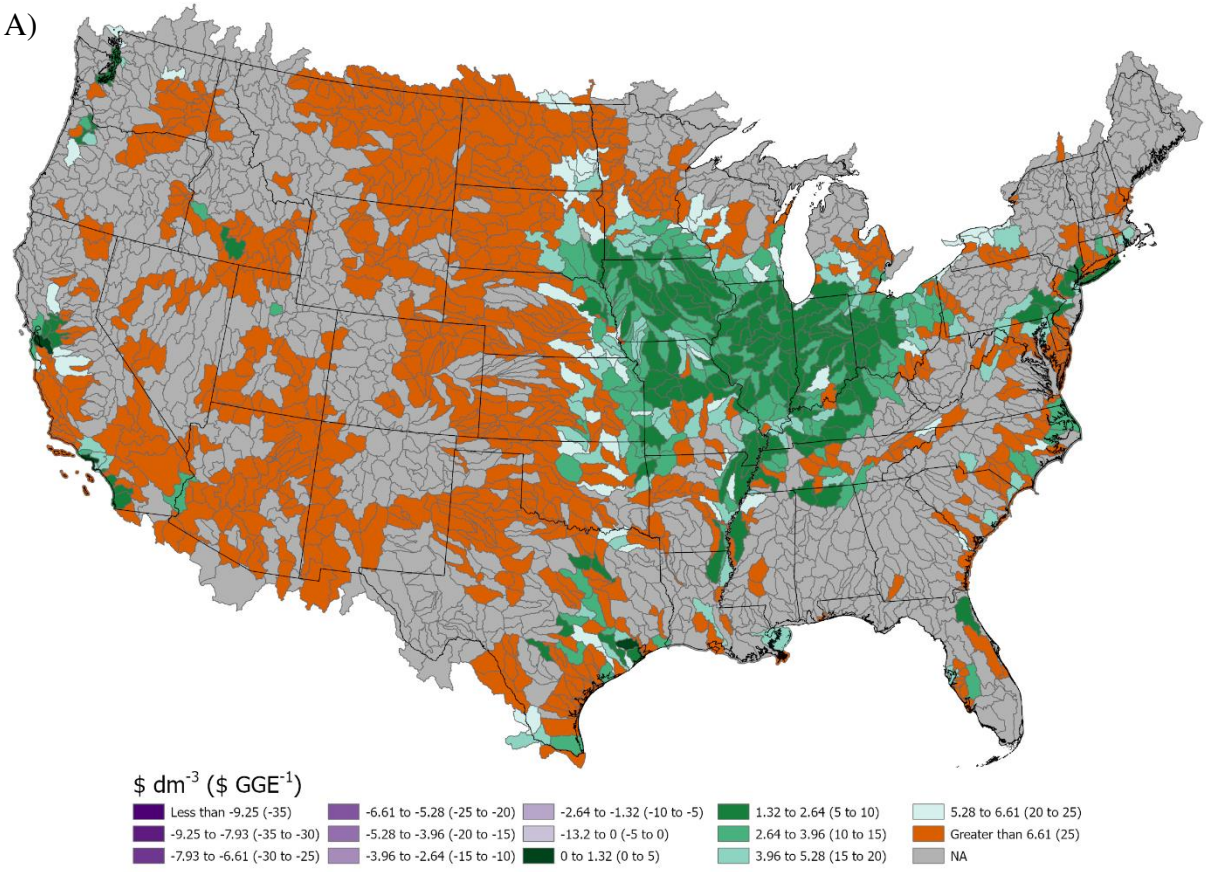
$ dm-3 ($ GGE-1)
Less than -9.25 (-35)
-9.25 to -7.93 (-35 to -30)
-7.93 to -6.61 (-30 to -25)
-6.61 to -5.28 (-25 to -20)
-5.28 to -3.96 (-20 to -15)
-3.96 to -2.64 (-15 to -10)
-2.64 to -1.32 (-10 to -5)
-13.2 to 0 (-5 to 0)
0 to 1.32 (0 to 5)
1.32 to 2.64 (5 to 10)
2.64 to 3.96 (10 to 15)
3.96 to 5.28 (15 to 20)
5.28 to 6.61 (20 to 25)
Greater than 6.61 (25)
NA

B)

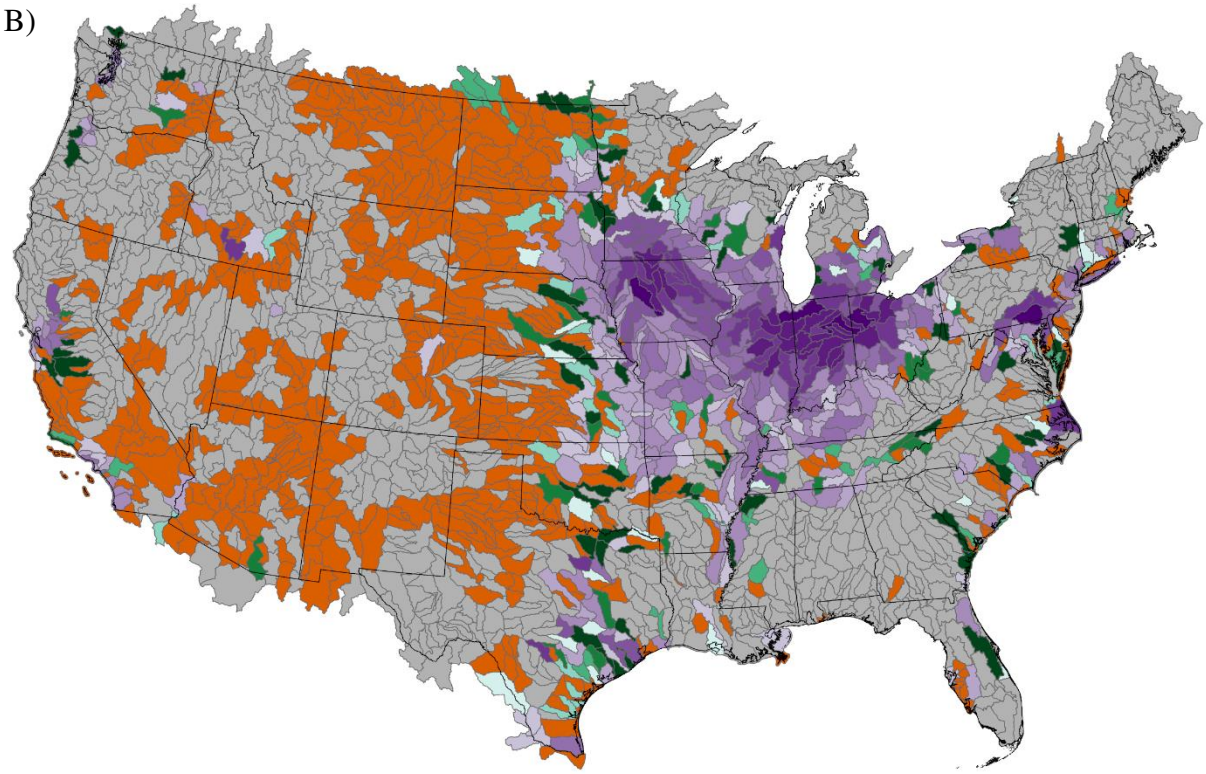

Fig. 6. Maps showing the renewable diesel minimum fuel selling price at the HUC8 level with a light efficiency of 2.8%, corresponding to a US maximum annual productivity of 25 g $m^{-2}day^{-1}$. Two levels of water quality trading (WQT) credits were used as subsidy inputs to the technoeconomic assessment model: (a) \$4.5 kg^{-1} (\$10 $lbs.^{-})^{1}$ and (b) \$45 kg^{-1} (\$100 $lbs.^{-})^{1}$. The values of the WQT represent a revenue in the cashflows for the mass of nitrogen and phosphorus removed from each HUC8 subbasin.

Chapter 4 – Conclusions

This study demonstrates a feasible path forward for deploying attached algae flow-ways to mitigate eutrophication while producing renewable diesel in the process. The baseline LCA in Santa Monica Bay, CA determined that this system is capable of meeting RFS mandates with a 71% reduction in life cycle GHG emissions. When compared to other biofuel pathways, this system reduced the eutrophication potential associated with diesel consumption. The economics of the baseline model show high feedstock prices as the limiting factor for feasible deployment of this novel biorefinery. Sensitivity analyses highlighted that reducing attached algae flow-way capital costs and improving algae productivities are crucial to reducing feedstock prices. Reductions in the renewable diesel MFSP are also possible by reducing the ash content of the algae and improving biocrude yields. However, these improvements may not be enough to make the renewable diesel competitive with conventional diesel. The scalability of the system is evaluated through coupling of the system with a geographically resolved growth model that remediates contaminated water systems. The HUC8- level TEA results show that increasing the productivities reduces the MFSP to a minimum of \$1.21 dm^{-3} (\$4.56 GGE^{-1}). The biofuel prices varied, but the highest concentration of ideal locations is found in the Midwest. Additionally, the economic impact of incorporating two different WQT credits is evaluated. Valuing the water remediating capabilities of the algae at \$45 kg^{-1} (\$100 lb^{-1}) results in negative renewable diesel prices illustrating the ability of the system to be economically viable without revenue from the fuels product. Successful deployment of this system is possible in most states when WQT credits

are considered. Future work is needed to understand the limitations imposed by the availability of land to support large attached algae flow-way modules.

Bibliography

[1] F.R. Pick, Blooming algae: A Canadian perspective on the rise of toxic cyanobacteria, Can. J. Fish. Aquat. Sci. 73 (2016) 1149–1158. https://doi.org/10.1139/cjfas-2015-0470.

[2] K.G. Sellner, G.J. Doucette, G.J. Kirkpatrick, Harmful algal blooms: Causes, impacts and detection, J. Ind. Microbiol. Biotechnol. 30 (2003) 383–406. https://doi.org/10.1007/s10295-003-0074-9.

[3] and A.E.W. M. F. Chislock, E. Doster, R. A. Zitomer, Eutrophication: Causes, Consequences, and Controls in Aquatic Ecosystems, Nature. (2013). https://www.nature.com/scitable/knowledge/library/eutrophication-causes-consequences-and-controls-in-aquatic-102364466/.

[4] G. Hallegraeff, D.M. Anderson, W. Hole, A. Cembella, Manual on Harmful Marine Micro Algae, in: United Nations Educational, Scientific and Cultural Organization, 2003: pp. 25–50.

[5] M.A. Sutton, A. Bleeker, M. Bekunda, B. Grizzetti, W. de Vries, H. van Grinsven, Y.P. Abrol, T. Adhya, G. Billen, E. Davidson, A. Datta, R. Diaz, J.W. Erisman, X. Liu, O. Oenema, C. Palm, N. Raghuram, S. Reis, R. Scholz, T. Sims, X. Yan, Y. Zhang, Our Nutrient World: The challenge to produce more food and energy with less pollution, 2013. https://library.wur.nl/WebQuery/wurpubs/reports/434951.

[6] M.R. Al Shehhi, I. Gherboudj, H. Ghedira, An overview of historical harmful algae blooms outbreaks in the Arabian Seas, Mar. Pollut. Bull. 86 (2014) 314–324. https://doi.org/10.1016/j.marpolbul.2014.06.048.

[7] Nutrient Pollution: Sources and Solutions, EPA. (2022). https://www.epa.gov/nutrientpollution/sources-and-solutions (accessed August 3, 2022).

[8] East Coast: Harmful Algal Blooms, NOAA. (2022). https://oceanservice.noaa.gov/hazards/hab/east-coast.html (accessed August 3, 2022).

[9] West Coast/Alaska: Harmful Algal Blooms, NOAA. (2022). https://oceanservice.noaa.gov/hazards/hab/west-coast.html (accessed August 3, 2022).

[10] Gulf of Mexico/Florida: Harmful Algal Blooms, NOAA. (2022). https://oceanservice.noaa.gov/hazards/hab/gulf-mexico.html (accessed August 3, 2022).

[11] Great Lakes: Harmful Algal Blooms, NOAA. (2022). https://oceanservice.noaa.gov/hazards/hab/great-lakes.html (accessed August 3, 2022).

[12] Nutrient Pollution: Harmful Algal Blooms, EPA. (2022). https://www.epa.gov/nutrientpollution/harmful-algal-blooms#:~:text=Harmful algal blooms are a,Algal blooms can be toxic. (accessed August 3, 2022).

[13] J.L. Dodds, Walter K, Eitzmann, T.J. Pilger, K.L. Pitts, A.J. Riley, J.T. Schloesser, D.J.

Thornbrugh, Policy Analysis Eutrophication of U . S . Freshwaters : Damages, 43 (2009).

[14] D.M. Anderson, Approaches to monitoring, control and management of harmful algal blooms (HABs), Ocean Coast. Manag. 52 (2009) 342–347. https://doi.org/10.1016/j.ocecoaman.2009.04.006.

[15] K.K. DeRose, R.W. Davis, E.A. Monroe, J.C. Quinn, Economic viability of proactive harmful algal bloom mitigation through attached algal growth, J. Great Lakes Res. 47 (2021) 1021–1032. https://doi.org/10.1016/j.jglr.2021.04.011.

[16] EPA, A Compilation of Cost Data Associated with the Impacts and Control of Nutrient Pollution, 2015. https://www.epa.gov/sites/default/files/2015-04/documents/nutrient-economics-report-2015.pdf.

[17] M. Munawar, M.A.J.Ã. Fitzpatrick, Eutrophication in three Canadian Areas of Concern : Phytoplankton and major nutrient interactions, Aquat. Ecosyst. Health Manag. 21 (2018) 421–437. https://doi.org/10.1080/14634988.2018.1530895.

[18] J.L. Graham, N.M. Dubrovsky, G.M. Foster, L.R. King, A. Loftin, B.H. Rosen, E.A. Stelzer, J.L. Graham, N.M. Dubrovsky, G.M. Foster, L.R. King, A. Loftin, B.H. Rosen, E.A. Stelzer, J.L. Graham, N.M. Dubrovsky, G.M. Foster, B.H. Rosen, E.A. Stelzer, L.R. King, K.A. Loftin, Cyanotoxin occurrence in large rivers of the United States Cyanotoxin occurrence in large rivers of the United States, 2041 (2020). https://doi.org/10.1080/20442041.2019.1700749.

[19] H. Liu, R. Brouwer, Incentivizing the future adoption of best management practices on agricultural land to protect water resources : The role of past participation and experiences, Ecol. Econ. 196 (2022) 107389. https://doi.org/10.1016/j.ecolecon.2022.107389.

[20] HydroMentia, S-154 Pilot Single Stage Algal Turf Scrubber ® (ATS TM) Final Report, 2005. https://hydromentia.com/resources/ats-library/.

[21] W.H. Adey, H.D. Laughinghouse, J.B. Miller, L.A.C. Hayek, J.G. Thompson, S. Bertman, K. Hampel, S. Puvanendran, Algal turf scrubber (ATS) floways on the Great Wicomico River, Chesapeake Bay: Productivity, algal community structure, substrate and chemistry1, J. Phycol. 49 (2013) 489–501. https://doi.org/10.1111/jpy.12056.

[22] W.H. Adey, P.C. Kangas, W. Mulbry, Algal turf scrubbing: Cleaning surface waters with solar energy while producing a biofuel, Bioscience. 61 (2011) 434–441. https://doi.org/10.1525/bio.2011.61.6.5.

[23] W. Mulbry, P. Kangas, S. Kondrad, Toward scrubbing the bay: Nutrient removal using small algal turf scrubbers on Chesapeake Bay tributaries, Ecol. Eng. 36 (2010) 536–541. https://doi.org/10.1016/j.ecoleng.2009.11.026.

[24] S. Kim, C. Quiroz-Arita, E.A. Monroe, A. Siccardi, J. Mitchell, N. Huysman, R.W. Davis, Application of attached algae flow-ways for coupling biomass production with the utilization of dilute non-point source nutrients in the Upper Laguna Madre, TX, Water Res. 191 (2021) 116816. https://doi.org/10.1016/j.watres.2021.116816.

[25] R. Davis, C. Kinchin, J. Markham, E.C.D. Tan, L.M.L. Laurens, Process Design and

Economics for the Conversion of Algal Biomass to Biofuels : Algal Biomass Fractionation to Lipid- Products Process Design and Economics for the Conversion of Algal Biomass to Biofuels : Algal Biomass Fractionation to Lipid- and Carbohyd, Nrel. (2014) NREL/TP-5100-62368.

[26] J.C. Quinn, A. Hanif, S. Sharvelle, T.H. Bradley, Microalgae to biofuels: Life cycle impacts of methane production of anaerobically digested lipid extracted algae, Bioresour. Technol. 171 (2014) 37–43. https://doi.org/10.1016/j.biortech.2014.08.037.

[27] J.C. Quinn, R. Davis, The potentials and challenges of algae based biofuels: A review of the techno-economic, life cycle, and resource assessment modeling, Bioresour. Technol. 184 (2015) 444–452. https://doi.org/10.1016/j.biortech.2014.10.075.

[28] J. Clippinger, R. Davis, J. Clippinger, R. Davis, Techno-Economic Assessment for Opportunities to Integrate Algae Farming with Wastewater Treatment Techno-Economic Assessment for Opportunities to Integrate Algae Farming with Wastewater Treatment, (2021).

[29] A. Singh, S.I. Olsen, A critical review of biochemical conversion, sustainability and life cycle assessment of algal biofuels, Appl. Energy. 88 (2011) 3548–3555. https://doi.org/10.1016/j.apenergy.2010.12.012.

[30] J. Barlow, R.C. Sims, J.C. Quinn, Techno-economic and life-cycle assessment of an attached growth algal biorefinery, Bioresour. Technol. 220 (2016) 360–368. https://doi.org/10.1016/j.biortech.2016.08.091.

[31] R. Pate, G. Klise, B. Wu, Resource demand implications for US algae biofuels production scale-up, Appl. Energy. 88 (2011) 3377–3388. https://doi.org/10.1016/j.apenergy.2011.04.023.

[32] K. DeRose, C. DeMill, R.W. Davis, J.C. Quinn, Integrated techno economic and life cycle assessment of the conversion of high productivity, low lipid algae to renewable fuels, Algal Res. 38 (2019) 101412. https://doi.org/10.1016/j.algal.2019.101412.

[33] D. Cordell, S. White, Peak phosphorus: Clarifying the key issues of a vigorous debate about long-term phosphorus security, Sustainability. 3 (2011) 2027–2049. https://doi.org/10.3390/su3102027.

[34] E. Lurie-Luke, Product and technology innovation: What can biomimicry inspire?, Biotechnol. Adv. 32 (2014) 1494–1505. https://doi.org/10.1016/j.biotechadv.2014.10.002.

[35] W. Adey, C. Luckett, K. Jensen, Phosphorus Removal from Natural Waters, Restor. Ecol. 1 (1993) 29–39.

[36] J.R.J. Ruppert J. Craggs, Walter H. Addey, Phosphorus removal from wastewater using an algal turf scrubber, Water Sci. Technol. (1996). https://doi.org/https://doi.org/10.1016/0273-1223(96)00354-X.

[37] J. Hoffman, R.C. Pate, T. Drennen, J.C. Quinn, Techno-economic assessment of open microalgae production systems, Algal Res. 23 (2017) 51–57. https://doi.org/10.1016/j.algal.2017.01.005.

[38] D. Hess, L.M. Wendt, B.D. Wahlen, J.E. Aston, H. Hu, J.C. Quinn, Techno-economic analysis of ash removal in biomass harvested from algal turf scrubbers, Biomass and Bioenergy. 123 (2019) 149–158. https://doi.org/10.1016/j.biombioe.2019.02.010.

[39] P.H. Chen, J.C. Quinn, Microalgae to biofuels through hydrothermal liquefaction: Open-source techno-economic analysis and life cycle assessment, Appl. Energy. 289 (2021) 116613. https://doi.org/10.1016/j.apenergy.2021.116613.

[40] D. Knorr, J. Lukas, P. Schoen, Production of Advanced Biofuels via Liquefaction. Hydrothermal Liquefaction Reactor Design, Contract. 303 (2013) 275–3000.

[41] S. Jones, Y. Zhu, D. Anderson, R.T. Hallen, D.C. Elliott, Process Design and Economics for the Conversion of Algal Biomass to Hydrocarbons : Whole Algae Hydrothermal Liquefaction and Upgrading, Pnnl. (2014) 1–69. http://www.pnnl.gov/main/publications/external/technical_reports/PNNL-23227.pdf.

[42] V.R.I. Anne Hoos, Spatially referenced models of streamflow and nitrogen, phosphorus, and suspended-sediment loads in the Southeastern United States, 2019. https://doi.org/https://doi.org/10.3133/sir20195135.

[43] S. Ator, Spatially referenced models of streamflow and nitrogen, phosphorus, and suspended-sediment loads in streams of the Northeastern United States, 2019. https://doi.org/https://doi.org/10.3133/sir20195118.

[44] D.S. Dale Robertson, Spatially referenced models of streamflow and nitrogen, phosphorus, and suspended-sediment loads in streams of the Midwestern United States, 2019. https://doi.org/https://doi.org/10.3133/sir20195114.

[45] D. Wise, Spatially referenced models of streamflow and nitrogen, phosphorus, and suspended-sediment loads in streams of the Pacific region of the United States, 2019. https://doi.org/https://doi.org/10.3133/sir20195112.

[46] O.M. Daniel Wise, David Anning, David, Spatially referenced models of streamflow and nitrogen, phosphorus, and suspended-sediment transport in streams of the southwestern United States, 2019. https://doi.org/https://doi.org/10.3133/sir20195106.

[47] S. Wilcox, W. Marion, Users manual for TMY3 data sets, Renew. Energy. (2008) 51. http://scholar.google.com/scholar?hl=en&btnG=Search&q=intitle:Users+Manual+for+TMY3+Data+Sets+Users+Manual+for+TMY3+Data+Sets#1%5Cnhttp://scholar.google.com/scholar?hl=en&btnG=Search&q=intitle:May.?Users+manual+for+TMY3+data+sets+users+manual+for+TMY3+dat.

[48] J.M. Greene, D. Quiroz, S. Compton, P.J. Lammers, J.C. Quinn, A validated thermal and biological model for predicting algal productivity in large scale outdoor cultivation systems, Algal Res. 54 (2021) 102224. https://doi.org/10.1016/j.algal.2021.102224.

[49] D. Quiroz, J.M. Greene, J. McGowen, J.C. Quinn, Geographical assessment of open pond algal productivity and evaporation losses across the United States, Algal Res. 60 (2021) 102483. https://doi.org/10.1016/j.algal.2021.102483.

[50] M. Arabi, R.S. Govindaraju, M.M. Hantush, A probabilistic approach for analysis of uncertainty in the evaluation of watershed management practices, J. Hydrol. 333 (2007)

459–471. https://doi.org/10.1016/j.jhydrol.2006.09.012.

[51] A. Beattie, W. Vermaas, A. Darzins, S.C. Holland, S. Li, J. Mcgowen, D. Nielsen, J.C. Quinn, M. Carlo, A probabilistic economic and environmental impact assessment of a cyanobacteria-based biorefinery, Algal Res. 59 (2021) 102454. https://doi.org/10.1016/j.algal.2021.102454.

[52] 92nd U.S. Congress, Federal Water Pollution Control Act Amendments of 1972, United States of America, 1972.

[53] EPA, NPDES Permit Writers' Manual, 2010. https://www.epa.gov/sites/default/files/2015-09/documents/pwm_2010.pdf.

[54] S. of C.S.W.R.C. Board, ORDER WQ 2012-0013, United States of America, 2012. https://www.waterboards.ca.gov/board_decisions/adopted_orders/water_quality/2012/wqo 2012_0013.pdf.

[55] EPA, State-Specific Water Quality Standards Effective under the Clean Water Act (CWA), U.S. Environ. Prot. Agency. (2022). https://www.epa.gov/wqs-tech/state-specific-water-quality-standards-effective-under-clean-water-act-cwa.

[56] United States Environmental Protection Agency, Nutrient Criteria Technical Guidance Manual. Rivers and Streams, Breeam Communities. (2000) 22, 56 of 222. www.epa.gov.

[57] J.W. Clune, J.K. Crawford, E.W. Boyer, Nitrogen and Phosphorus Concentration Thresholds, Water. (2020) 1–13.

[58] K.M. Weyer, D.R. Bush, A. Darzins, B.D. Willson, Theoretical maximum algal oil production, Bioenergy Res. 3 (2010) 204–213. https://doi.org/10.1007/s12155-009-9046-x.

[59] R. Davis, J. Markham, C. Kinchin, N. Grundl, E. Tan, D. Humbird, Process design and economics for the production of algal biomass: algal biomass production in open pond systems and processing through dewatering for downstream conversion, Natl. Renew. Energy Lab. (2016) 128. www.nrel.gov/publications.

[60] T. Takahashi, W.S. Broecker, S. Langer, Redfield ratio based on chemical data from isopycnal surfaces., J. Geophys. Res. 90 (1985) 6907–6924. https://doi.org/10.1029/JC090iC04p06907.

[61] Nature, The Redfield ratio at 80, Nat. Geosci. (2014). https://www.nature.com/collections/fncspbsnmk#:~:text=In 1934%2C Alfred Redfield discovered,and in dissolved nutrient pools.

[62] Population of the largest metropolitan areas in the U.S. as of 2019, Statista. (2019). https://www.statista.com/statistics/183600/population-of-metropolitan-areas-in-the-us/ (accessed December 4, 2022).

[63] Uc. Argonne, GREET 1, (2021). https://greet.es.anl.gov/.

[64] G. Wernet, C. Bauer, B. Steubing, J. Reinhard, E. Moreno-Ruiz, B. Weidema, The ecoinvent database version 3 (part I): overview and methodology, Int. J. Life Cycle

Assess. 21 (2016) 1218–1230. https://doi.org/10.1007/s11367-016-1087-8.

[65] GreenDelta, openLCA, (2020). https://openlca.org/.

[66] A. Mehmeti, A. Angelis-Dimakis, G. Arampatzis, S.J. McPhail, S. Ulgiati, Life cycle assessment and water footprint of hydrogen production methods: From conventional to emerging technologies, Environ. - MDPI. 5 (2018) 1–19. https://doi.org/10.3390/environments5020024.

[67] J. S., Chemical Engineering Plant Cost Index Annual Average, Chem. Eng. (2019). https://www.chemengonline.com/2019-chemical-engineering-plant-cost-index-annual-average/ (accessed September 5, 2022).

[68] C.B. Program, Cost Effectiveness of BMPs, 2020. https://cast.chesapeakebay.net/Documentation/CostProfiles.

[69] A.B. Jeff Thomas, Personal communication with EPRI and First Climate, Electr. Power Reseach Institute, First Clim. (2021).

[70] K.S. Blunk, A Primer on Water Quality Credit Trading in the Mid-Atlantic Region, PennState Ext. (2006). https://extension.psu.edu/a-primer-on-water-quality-credit-trading-in-the-mid-atlantic-region.

[71] H. Hagemann, Researchers, robots dive into what makes some bay algal blooms toxic, St. Cruz Sentin. (2021). https://www.santacruzsentinel.com/2021/04/24/researchers-robots-dive-into-what-makes-some-bay-algal-blooms-toxic/ (accessed December 4, 2022).

[72] Overview for Renewable Fuel Standard, EPA. (2022). https://www.epa.gov/renewable-fuel-standard-program/overview-renewable-fuel-standard (accessed October 4, 2022).

[73] J.R. Cruce, A. Beattie, P. Chen, D. Quiroz, M. Somers, S. Compton, K. DeRose, B. Beckstrom, J.C. Quinn, Driving toward sustainable algal fuels: A harmonization of techno-economic and life cycle assessments, Algal Res. 54 (2021) 102169. https://doi.org/10.1016/j.algal.2020.102169.

[74] J. Bare, Tool for the Reduction and Assessment of Chemical and Other Environmental Impacts (TRACI) version 2.1, U.S. Environ. Prot. Agency. 600/R–12/5 (2012) 24.

[75] E.P. Bennion, D.M. Ginosar, J. Moses, F. Agblevor, J.C. Quinn, Lifecycle assessment of microalgae to biofuel: Comparison of thermochemical processing pathways, Appl. Energy. 154 (2015) 1062–1071. https://doi.org/10.1016/j.apenergy.2014.12.009.

[76] L. Batan, J. Quinn, B. Willson, T. Bradley, Net energy and greenhouse gas emission evaluation of biodiesel derived from microalgae, Environ. Sci. Technol. 44 (2010) 7975–7980. https://doi.org/10.1021/es102052y.

[77] X. Liu, B. Saydah, P. Eranki, L.M. Colosi, B. Greg Mitchell, J. Rhodes, A.F. Clarens, Pilot-scale data provide enhanced estimates of the life cycle energy and emissions profile of algae biofuels produced via hydrothermal liquefaction, Bioresour. Technol. 148 (2013) 163–171. https://doi.org/10.1016/j.biortech.2013.08.112.

[78] P. Fantke, M. Bijster, C. Guignard, M.Z. Hauschild, M.A.J. Huijbregts, O. Jolliet, A.

Kounina, V. Magaud, M. Margni, T.E. McKone, L. Posthuma, R.K. Rosenbaum, D. van de Meent, R. van Zelm, USEtox 2.0 Documentation (Version 1), 2017. https://doi.org/10.11581/DTU:00000011.

[79] Ground-level Ozone, Basic Information, EPA. (2008). http://www.epa.gov/air/ozonepollution/basic.html (accessed December 4, 2022).

[80] Inhalable Particulate Matter and Health (PM2.5 and PM10), Calif. Air Resour. Board. (2022). https://ww2.arb.ca.gov/resources/inhalable-particulate-matter-and-health (accessed September 6, 2022).

[81] P.H. Chen, J.L. Venegas Jimenez, S.M. Rowland, J.C. Quinn, L.M.L. Laurens, Nutrient recycle from algae hydrothermal liquefaction aqueous phase through a novel selective remediation approach, Algal Res. 46 (2020) 101776. https://doi.org/10.1016/j.algal.2019.101776.

[82] Y. Zhu, S.B. Jones, A.J. Schmidt, K.O. Albrecht, S.J. Edmundson, D.B. Anderson, Techno-economic analysis of alternative aqueous phase treatment methods for microalgae hydrothermal liquefaction and biocrude upgrading system, Algal Res. 39 (2019) 101467. https://doi.org/10.1016/j.algal.2019.101467.

[83] U. Jena, K.C. Das, J.R. Kastner, Effect of operating conditions of thermochemical liquefaction on biocrude production from Spirulina platensis, Bioresour. Technol. 102 (2011) 6221–6229. https://doi.org/10.1016/j.biortech.2011.02.057.

[84] P.J. Valdez, M.C. Nelson, H.Y. Wang, X.N. Lin, P.E. Savage, Hydrothermal liquefaction of Nannochloropsis sp.: Systematic study of process variables and analysis of the product fractions, Biomass and Bioenergy. 46 (2012) 317–331. https://doi.org/10.1016/j.biombioe.2012.08.009.

[85] D. López Barreiro, C. Zamalloa, N. Boon, W. Vyverman, F. Ronsse, W. Brilman, W. Prins, Influence of strain-specific parameters on hydrothermal liquefaction of microalgae, Bioresour. Technol. 146 (2013) 463–471. https://doi.org/10.1016/j.biortech.2013.07.123.

[86] D.C. Elliott, T.R. Hart, A.J. Schmidt, G.G. Neuenschwander, L.J. Rotness, M. V. Olarte, A.H. Zacher, K.O. Albrecht, R.T. Hallen, J.E. Holladay, Process development for hydrothermal liquefaction of algae feedstocks in a continuous-flow reactor, Algal Res. 2 (2013) 445–454. https://doi.org/10.1016/j.algal.2013.08.005.

[87] D. Xu, P.E. Savage, Effect of reaction time and algae loading on water-soluble and insoluble biocrude fractions from hydrothermal liquefaction of algae, Algal Res. 12 (2015) 60–67. https://doi.org/10.1016/j.algal.2015.08.005.

[88] Y. Zhu, K.O. Albrecht, D.C. Elliott, R.T. Hallen, S.B. Jones, Development of hydrothermal liquefaction and upgrading technologies for lipid-extracted algae conversion to liquid fuels, Algal Res. 2 (2013) 455–464. https://doi.org/10.1016/j.algal.2013.07.003.

[89] N. Neveux, A.K.L. Yuen, C. Jazrawi, M. Magnusson, B.S. Haynes, A.F. Masters, A. Montoya, N.A. Paul, T. Maschmeyer, R. de Nys, Biocrude yield and productivity from the hydrothermal liquefaction of marine and freshwater green macroalgae, Bioresour. Technol. 155 (2014) 334–341. https://doi.org/10.1016/j.biortech.2013.12.083.

[90] V. Vecchi, S. Barera, R. Bassi, L. Dall'osto, Potential and challenges of improving photosynthesis in algae, Plants. 9 (2020). https://doi.org/10.3390/plants9010067.

[91] UN, Food and Agriculture Organization of the United Nations, FAO Stat. Databases. (2017). http://faostat.fao.org.

Appendix A

1. Water quality data

Data from the USGS Spatially Referenced Regression on Watershed attributes (SPARROW) model was used to determine nutrient impairment in each HUC8 subbasin in the contiguous US [1–5]. Total nitrogen (TN) concentrations, total phosphorus (TP) concentrations and TN to TP ratios from the SPARROW model data are mapped below

Appendix A 1. Total nitrogen (TN) concentrations of all 2,112 HUC8 subbasins. Southern Florida was not included in the USGS data set and appears as NA.

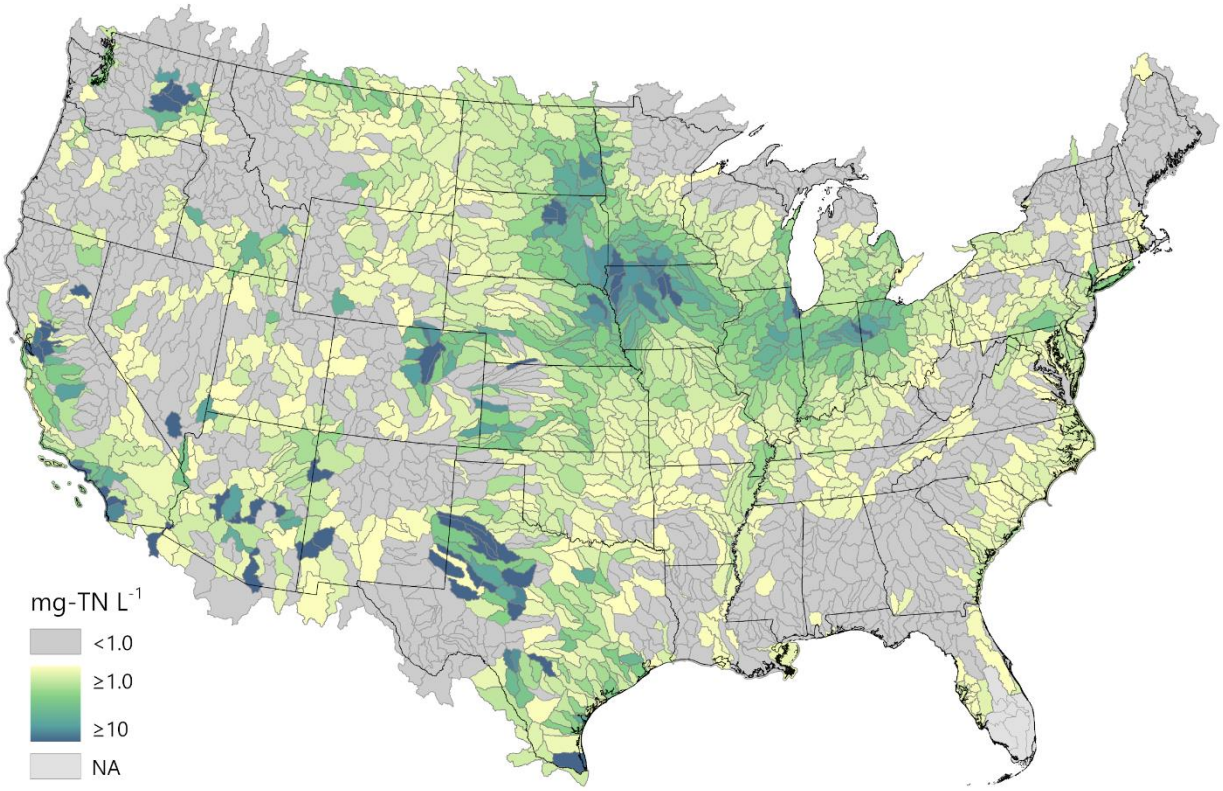

Appendix A 2. Total phosphorus (TP) concentrations of all 2,112 HUC8 subbasins. Southern Florida was not included in the USGS data set and appears as NA.

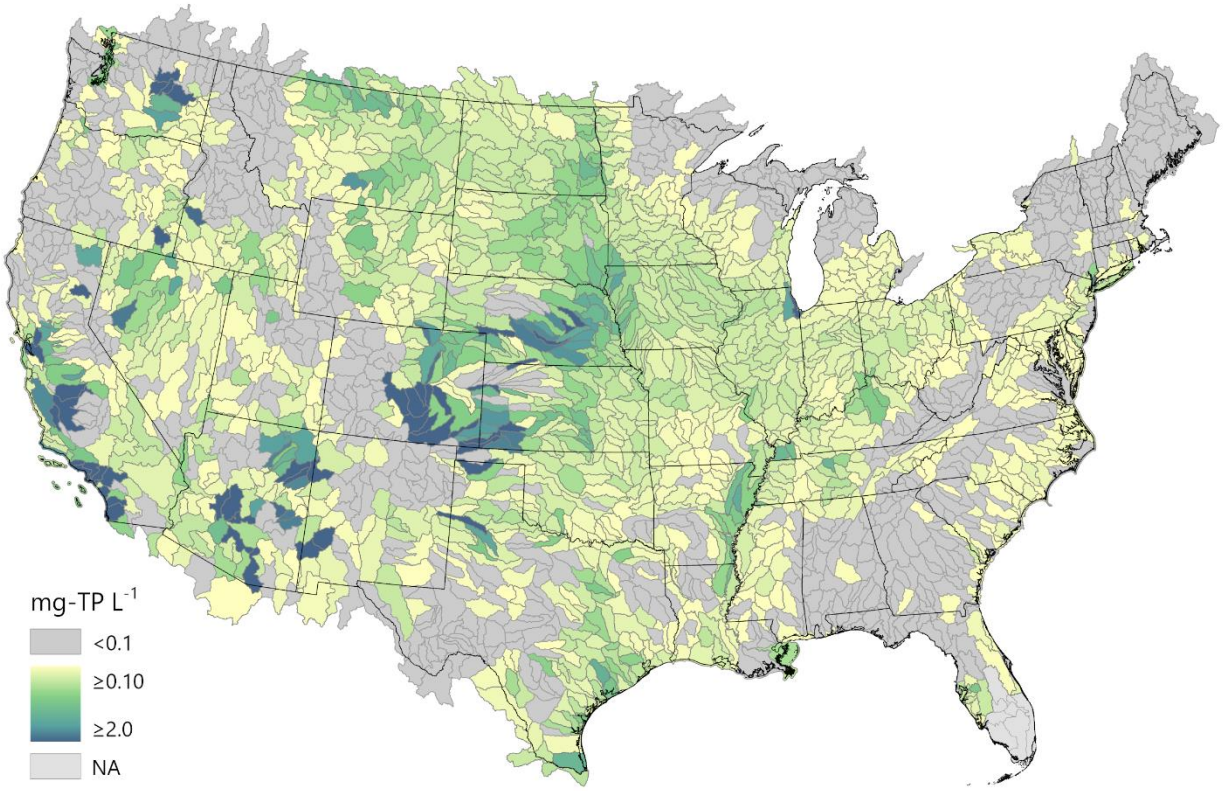

Appendix A 3. TN to TP ratios of all 2,112 HUC8 subbasins. Southern Florida was not included in the USGS data set and appears as NA.

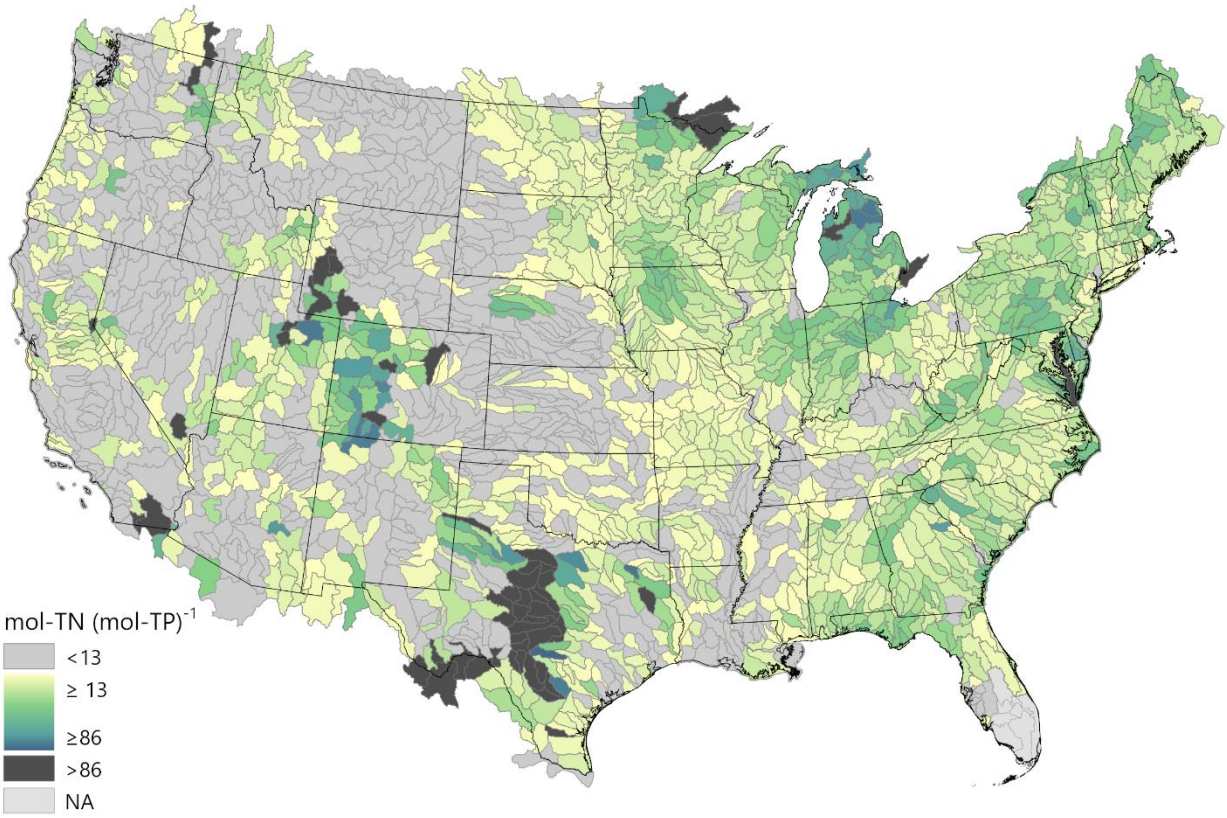

2. Operational days data

Appendix A 4. Operational days of all 2,112 HUC8 subbasins.

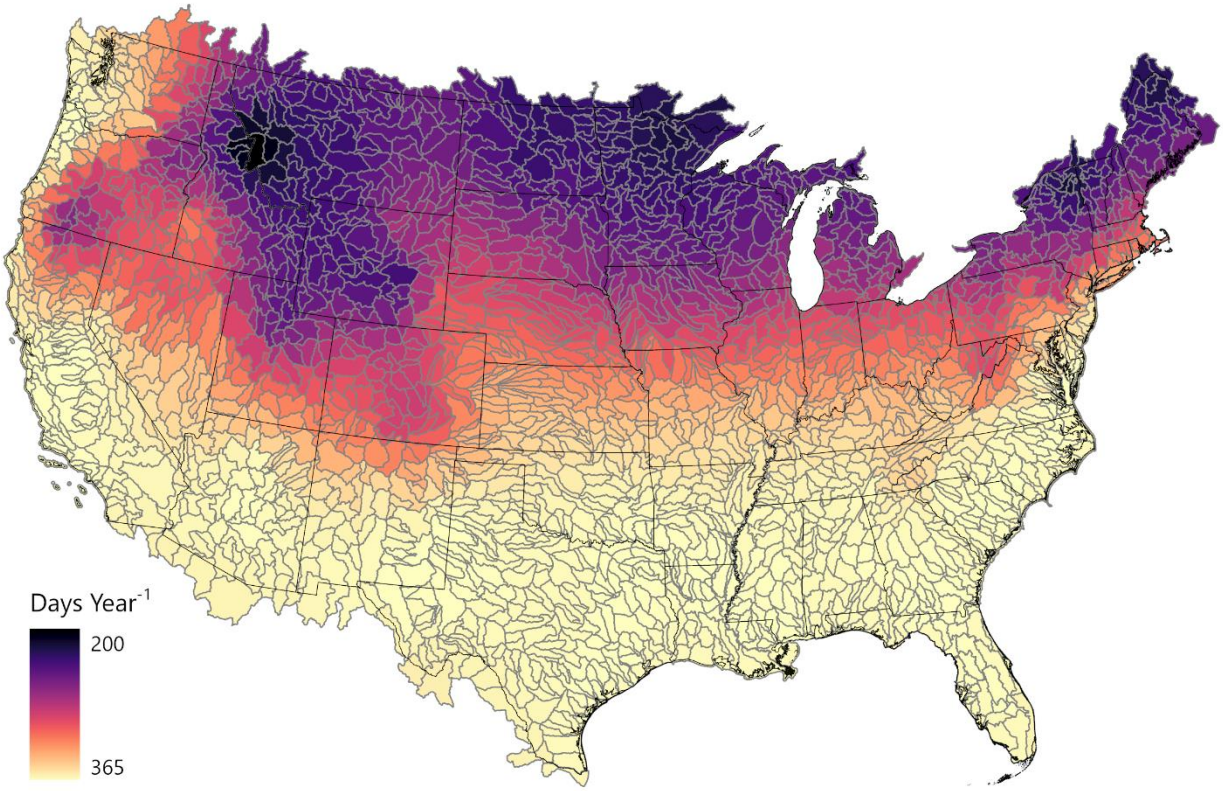

3. 1st order algae growth model

Algae productivities were estimated with the following equation:

$$P\left[\frac{g}{m^2\ day}\right] = \frac{0.458 * GHI\left[\frac{kJ}{m^2\ day}\right]}{22\left[\frac{kJ}{g}\right]} * \eta$$

where P is algae productivity in g m^{-2} day^{-1}, 0.458 is the fraction of full spectrum radiation that is photosynthetically active radiation [6], GHI is the full spectrum radiation in kJ m^{-2} day^{-1}, 22 is the energy density of the algae biomass in kJ g^{-1} [7], and η is the photosynthetic light efficiency of the algae.

The following field trail data was leveraged to validate the 1st order growth model [8,9]:

Appendix A 5. Field trail data acquired by Sandia National Laboratories in Laguna Madre, TX. The Global Horizontal Irradiance (GHI) was converted from W m-2 day-1 to kJ m-2 day-1. The productivities were converted into equivalent units and divided by the GHI to determine the photosynthetic light efficiency.

Date	GHI [kJ m-2 day -1]	Productivity [g m-2 day-1]	Productivity [kJ m-2 day-1]	Light efficiency
17-Jan	12,850	3.5	77.3	0.6%
24-Jan	9,391	2.2	48.2	0.5%
31-Jan	10,905	1.7	38.3	0.4%
7-Feb	8,514	2.6	57.2	0.7%
21-Feb	14,618	6.9	150.9	1.0%
28-Feb	11,223	8.0	174.9	1.6%
7-Mar	15,384	11.2	247.1	1.6%
14-Mar	12,874	11.9	261.4	2.0%
21-Mar	17,677	16.2	355.7	2.0%
28-Mar	15,114	12.8	280.9	1.9%
4-Apr	18,241	13.6	298.5	1.6%
11-Apr	14,160	3.8	82.5	0.6%
18-Apr	21,616	9.0	198.4	0.9%
25-Apr	15,950	13.6	298.1	1.9%
2-May	13,000	14.6	321.4	2.5%
9-May	20,293	16.0	351.6	1.7%
16-May	20,796	9.8	216.0	1.0%
30-May	22,250	3.7	81.4	0.4%
6-Jun	21,863	9.8	215.6	1.0%
13-Jun	20,386	9.8	214.7	1.1%
20-Jun	13,864	22.1	486.0	3.5%
			avg	**1.4%**

After calibrating the growth model, three light efficiencies (1.4%, 2.8% and 4.5%) predicted the productivities across all subbasins in the contiguous US. This translates to three US maximum annual productivities for the attached algae flow-ways: 12.4 g m^{-2} day^{-1}, 25 g m^{-2} day^{-1} and 40 g m^{-2} day^{-1}.The resulting productivity maps are shown below.

Appendix A 6. Geographically-resolved annual average algae productivities assuming a light efficiency of 1.4%.

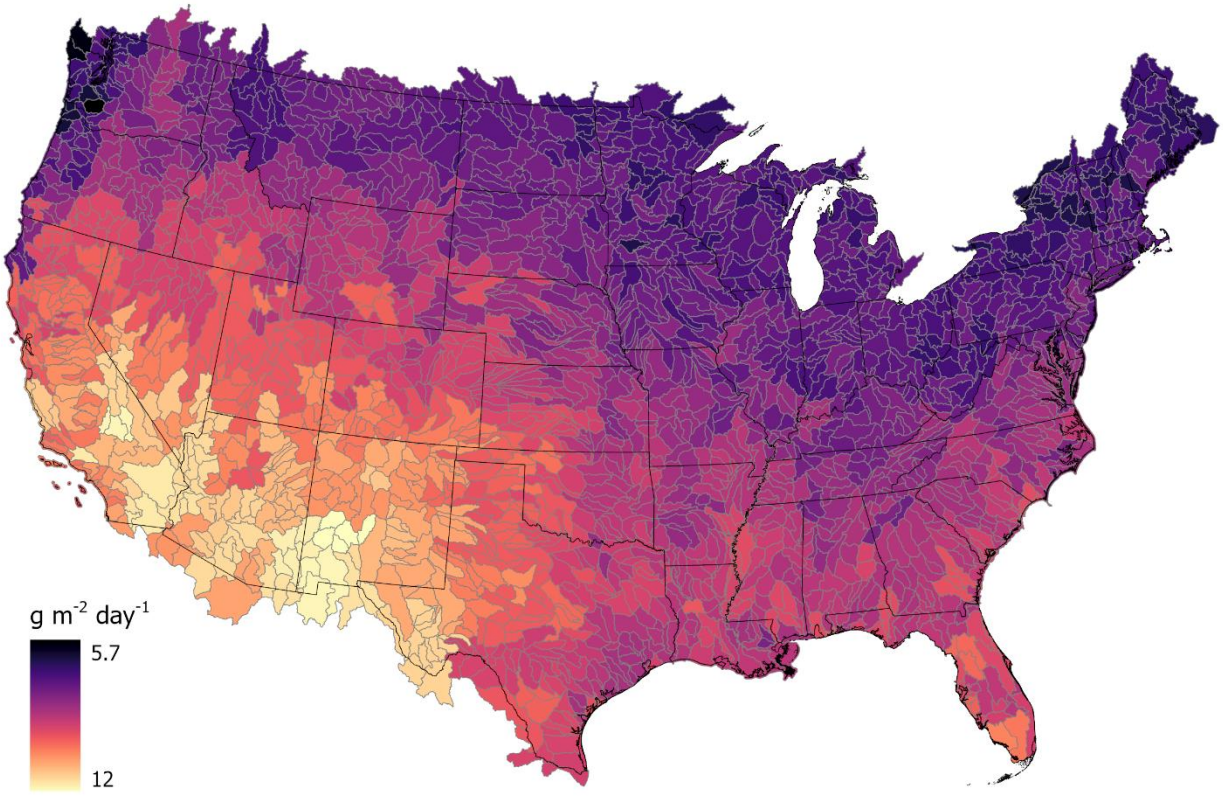

Appendix A 7. Geographically-resolved annual average algae productivities assuming a light efficiency of 2.8%.

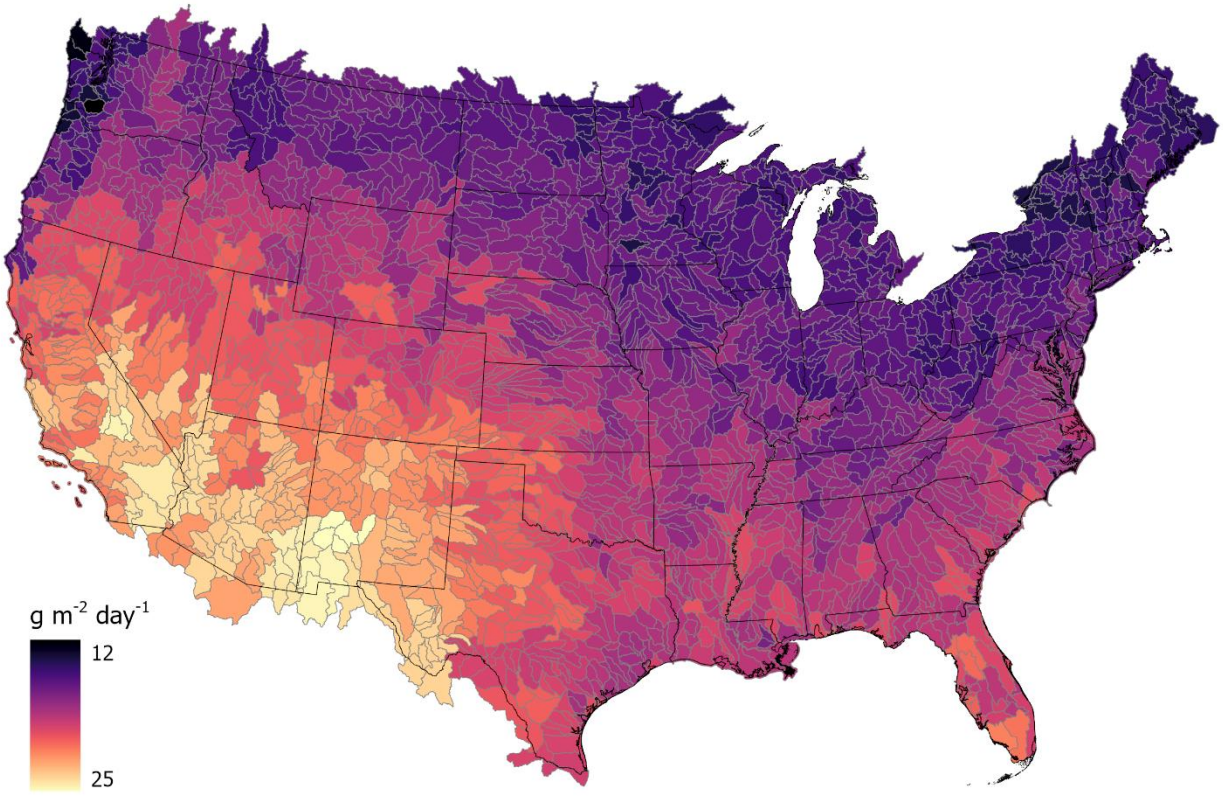

Appendix A 8. Geographically-resolved annual average algae productivities assuming a light efficiency of 4.5%.

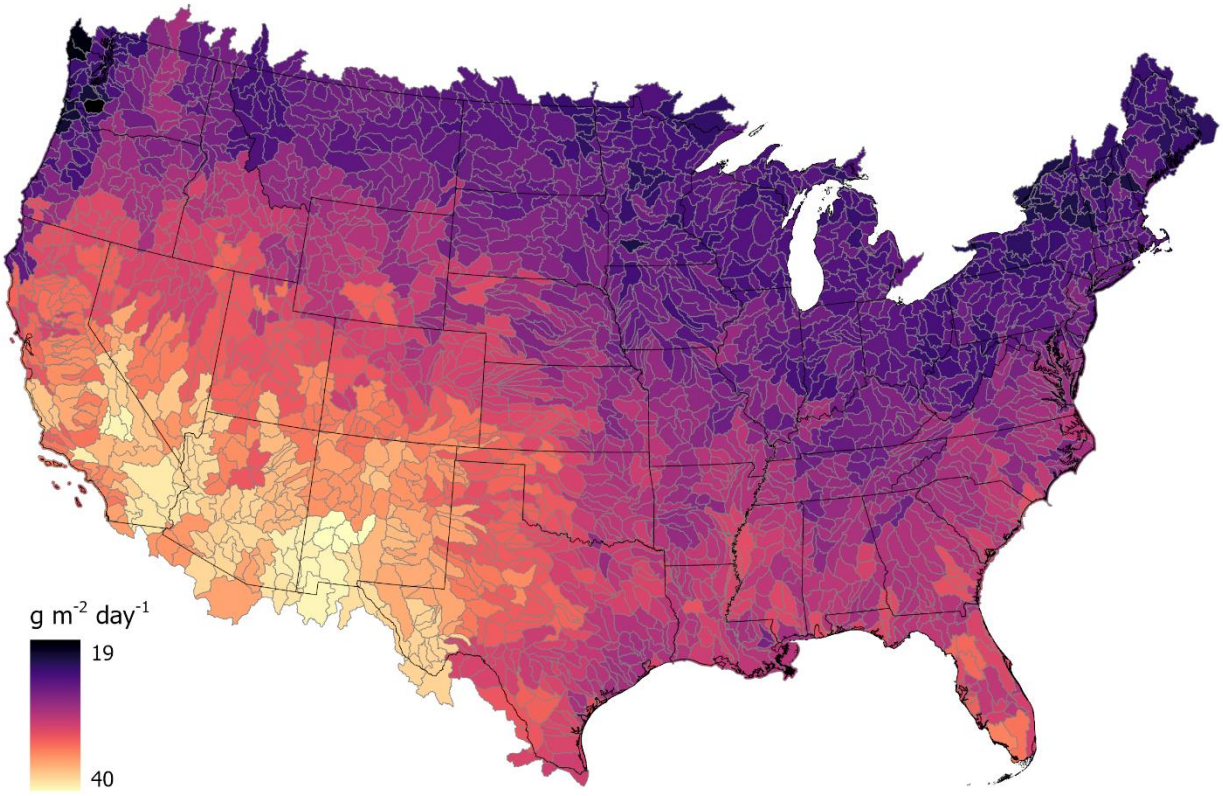

4. Variable algae composition

Linear regression was used to fit coefficients to polynomial equations that predict the composition of nitrogen and phosphorus in the algae biomass as a function of the inflow TN:TP ratio. Constraints were applied to ensure that the composition at an inflow TN:TP ratio of 13:1 was equivalent to the N-limiting algae composition and that the composition at an inflow TN:TP ratio of 86:1 was equivalent to the P-limiting algae composition. The following equations were estimate the composition of nitrogen and phosphorus in the harvested algae:

$$x_N = f\left(\frac{TN}{TP}\right) = -4.290E-05 * \left(\frac{TN}{TP}\right)^2 + 4.625E-03 * \left(\frac{TN}{TP}\right) + 4.749E-05$$

$$x_P = f\left(\frac{TN}{TP}\right) = 3.936E-10 * \left(\frac{TN}{TP}\right)^2 + 1.023E-02$$

where x_N is the mass fraction of nitrogen in the algae biomass and x_P is the mass fraction of phosphorus in the algae biomass. The variable composition plots are shown below. A reference line of the resulting algae N:P ratio versus inflow TN:TP ratio is also plotted.

Appendix A 9. Inflow total nitrogen (TN) to total phosphorus (TP) ratio versus the mass fraction of nitrogen and phosphorus in the algae biomass. A secondary axis shows the nitrogen to phosphorus ratio of the algae.

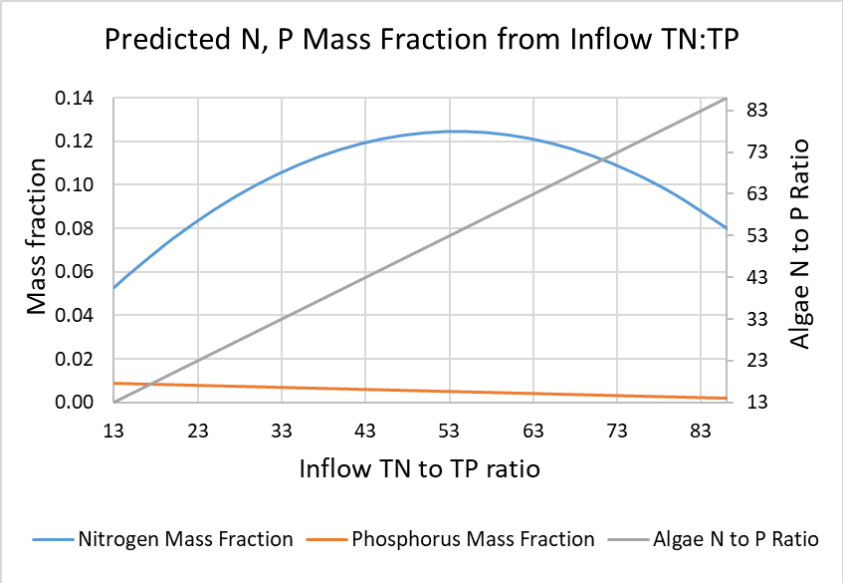

5. Life cycle analysis

Appendix A 10. Summary of TRACI 2.1 total environmental impacts of renewable diesel compared to conventional diesel and soy biodiesel on a well-to-wheels (WTW) basis.

Impact category	**Algal Renewable Diesel**	**Soy Biodiesel** [10,11]	**Conventional Diesel** [10,11]	**Units [per MJ fuel]**
Acidification	1.5×10^{-5}	1.2×10^{-4}	1.4×10^{-4}	kg SO_2 eq
Ecotoxicity	3.5×10^{-2}	7.1×10^{-2}	1.9×10^{-2}	CTUe
Eutrophication	1.3×10^{-5}	7.1×10^{-5}	4.0×10^{-5}	kg N eq
Global Warming Potential (GWP)	2.5×10^{-2}	1.0×10^{-1}	8.8×10^{-2}	kg CO_2 eq
Human health (carcinogenic)	2.5×10^{-10}	7.5×10^{-10}	3.7×10^{-10}	CTUh
Human health (non-carcinogenic)	1.6×10^{-9}	2.8×10^{-9}	7.7×10^{-10}	CTUh
Ozone depletion	3.7×10^{-9}	2.8×10^{-9}	2.0×10^{-8}	kg CFC-11 eq
Photochemical ozone formation	1.2×10^{-3}	2.6×10^{-3}	2.0×10^{-3}	kg O_3 eq
Fossil fuel depletion	2.8×10^{-1}	2.6×10^{-2}	1.7×10^{-1}	MJ surplus
Respiratory effects	1.5×10^{-5}	2.3×10^{-5}	1.6×10^{-5}	kg PM2.5 eq
Net Energy Ratio (NER)	3.3×10^{-1}	1.6×10^{0}	1.9×10^{-1}	MJ

The following contains the calculations used to determine the acidification potential (AP) for a pH change in the source waters from an attached algae flow-way. Two pH changes were investigated: 1) a pH change from 7 to 9; and 2) a pH change from 7 to 8. The Acidification of sulfur dioxide was found from Heijungs et al. (1992) [12]. Assume the flow rate of water through the Santa Monica Bay, CA subbasin is 472 MGD ($7.43*10^7$ L hr^{-1}) and the total fuel production is 234,238 MJ hr^{-1}.

1).

$$pH = -\log([H^+]) \rightarrow [H^+] = 10^{-pH}$$

$$\Delta pH = 7 - 9 = -2 \rightarrow \Delta[H^+] = 10^2 = 100\ mol\ L^{-1}$$

$$SO_2 + H_2O + O_3 \leftrightarrow 2H^+ + SO_4^{2-} + O_2$$

$$SO_{2-eq}\ emissions = \left(\frac{100\ mol\ H^+}{L}\right)\left(\frac{1\ mol\ SO_2}{2\ mol\ H^+}\right)\left(\frac{64.07\ g\ SO_2}{1\ mol\ SO_2}\right)\left(\frac{1\ kg}{10^3\ g}\right)\left(\frac{7.43 * 10^7\ L}{hr}\right)$$

$$= 2.38 * 10^8\ kg\ SO_{2-eq}\ hr^{-1}$$

$$AP = \frac{2.38 * 10^8\ kg\ SO_2\ hr^{-1}}{234{,}238\ MJ\ hr^{-1}} = 1{,}020\ kg\ SO_{2-eq}\ MJ^{-1}$$

2).

$$\Delta[H^+] = 10^1 = 10\ mol\ L^{-1}$$

$$SO_{2-eq}\ emissions = 2.38 * 10^7\ kg\ SO_{2-eq}\ hr^{-1}$$

$$AP = 102\ kg\ SO_{2-eq}\ MJ^{-1}$$

6. Bioenergy Technology Office cost assumptions

Appendix A 11. "Nth-of-a-kind plant" assumptions utilized in the discounted cashflow rate of return economic model to determine the minimum price of the biomass and the renewable diesel. The on-stream factor is a variable in the process model, see section 2.1.3. for more details.

Parameter	Standard Value
Internal rate of return	10%
Plant financing debt / equity	60% / 40%
Plant life	30 years
Income tax rate	35%
Interest rate	8.0% annual
Debt financing term	10 years
Depreciation schedule	7-year modified accelerated cost recovery system (MACRS)
Construction period	8% year 1 60% year 2 32% year 3
Plant salvage value	None
Start-up time	6 months
Start-up revenue and costs	50% revenue 75% variable costs 100% fixed costs
On-stream factor	Variable
Indirect capital	60% of total installed capital
Base costs year	2018

7. Cost estimates

Appendix A 12. Attached algae flow-way capital (CAPEX) and operational (OPEX) expenses. Costs are listed in 2018 $.

Variable	Value	Units	Source
CAPEX			
Growth System	$47,446	$ $acre^{-1}$	[13]
Harvest Equipment	$5,391	$ $acre^{-1}$	[13]
Land	$2,233	$ $acre^{-1}$	[14]
OPEX			
Pump energy use	0.006061	kW gpm^{-1}	[13]
Electricity	$0.036	$ kWh^{-1}	[15]
Additional energy use	10%	% of pump electricity use	[13]
Labor	$1,398	$ $acre^{-1}$	[13]
Harvesting	$646	$ $acre^{-1}$	[13]
Maintenance	1.6%	% of CAPEX	[13]

Appendix A 13. Equipment costs associated with the HTL system [16,17]. The costs are shown in 2018 $ and the results are representative of the Santa Monica Bay, CA HUC8 subbasin with a US maximum annual productivity of 25 g m^{-2} day^{-1}.

Equipment Title	Number Required	Quote Cost	Year of Quote	Scaling Variable	Units	Scaling Exponent	Installation Factor	Size Ratio	Scaled Purchase Cost	Purchase Cost in Project Year	Installed Cost in Project Year
Ash Reduction											
De-ash tank	2	$162,000	2005	1	Unit	1	1.14	1	$324,000	$416,285	$474,565
Filter press	1	$5,300	2010	98.01	$m^3 hr^{-1}$	1	1.8	98.0	$519,462	$570,236	$1,026,425
De-ash pump	4	$35,400	2010	45,881	kg hr^{-1}	.6	2.3	0.12	$39,025	$42,840	$98,531
								Ash Reduction Totals	$882,487	$1,029,361	$1,599,521
Hydrothermal Liquefaction											
First feed preheater	1	$44,604,000	2012	2,741	ft^2	0.7	2.2	0.06	$5,863,201	$6,048,746	$13,307,241
Second feed preheater	1	$31,860,000	2012	1,963	ft^2	0.7	2.2	0.06	$4,195,931	$4,328,714	$9,523,170
Feed recycle heat exchanger	1	$2,948,000	2012	3,654	ft^2	0.7	2.2	0.81	$2,548,343	$2,628,987	$5,783,771
Final feed heater	1	$998,850	2012	2,086	ft^2	0.7	2.2	0.35	$474,968	$489,999	$1,077,997
HTL reactor	1	$272,788	2013	7,848	ft	1.0	2.0	16.35	$4,460,054	$4,741,510	$9,483,020
Reactor gas KO drum	1	$5,600,000	2012	1	ft^3	0.7	2.0	1.00	$5,600,000	$5,777,215	$11,554,430
Solids filter	1	$1,311,000	2011	1,001	gpm	0.6	1.7	0.27	$599,266	$617,069	$1,049,017
Separator	1	$3,565,000	2011	1,001	gpm	0.7	2.0	0.27	$1,430,252	$1,472,742	$2,945,484
Bio-oil heat recovery steam generator	1	$102,000	2012	42	ft^2	0.7	2.2	0.05	$12,243	$12,630	$27,786
								Hydrothermal Liquefaction Totals	$25,184,258	$26,117,611	$54,751,917
Upgrading											
Hydrotreater reactor, vessels, columns	1	$27,000,000	2007	1,527	bpd	0.75	1.51	0.23	$9,087,278	$10,344,541	$15,620,256
Hydrogen compressor	1	$1,385,600	2011	3.2	MMscfd H2	0.80	1.10	0.19	$365,202	$376,052	$413,657
Hydrogen recycle PSA	1	$1,750,000	2004	3.2	MMscfd H2	0.80	2.47	0.19	$9,087,278	$622,184	$1,536,793
Hydrocracker unit and auxiliaries	1	$25,000,000	2007	148.3	bpd	0.75	1.51	0.07	$3,307,899	$3,765,561	$5,685,997
								Upgrading Totals	$13,221,628	$15,108,337	$23,256,704
Utilities											
Hot oil system package	1	$1,200,500	2012	20	MMBtu hr^{-1}	0.6	1.8	0.33	$612,790	$632,182	$1,137,928
Hot oil	1	$2,101,710	2012	23,200	gal	1.0	1.0	1.00	$2,101,710	$2,168,220	$2,168,220
Cooling tower system	1	$2,000,000	2009	64,730	lb hr^{-1}	0.60	2.95	0.002	$45,352	$52,639	$155,287
Cooling water pump	1	$445,700	2009	64,730	lb hr^{-1}	0.60	2.95	0.002	$10,107	$11,730	$34,606
Plant air compressor	1	$32,376	2002	14.7	ton day^{-1}	0.34	2.95	0.007	$6,089	$9,307	$27,456
Hydraulic truck dump with scale	1	$80,000	1998	14.7	ton day^{-1}	0.60	2.95	0.007	$4,193	$6,491	$19,149
Firewater pump	1	$184,000	1997	14.7	ton day^{-1}	0.79	2.95	0.007	$3,791	$5,917	$17,456
Instrument air dryer	1	$8,349	2002	14.7	ton day^{-1}	0.60	2.95	0.007	$438	$668	$1,973
Plant air receiver	1	$7,003	2002	14.7	ton day^{-1}	0.72	2.95	0.007	$204	$311	$918
Firewater storage tank	1	$166,100	1997	14.7	ton day^{-1}	0.51	2.95	0.007	$13,549	$21,147	$62,385
HTL oil intermediate storage (3 day)	1	$470,000	2005	192,441	gal	0.65	2.95	0.182	$155,340	$199,586	$588,779
Naphtha storage (3 day)	1	$320,384	2005	21,646	gal	0.65	2.95	0.039	$38,758	$49,797	$146,903
Biodiesel storage (3 day)	1	$320,384	2005	97,513	gal	0.65	2.95	0.175	$103,098	$132,463	$390,767
								Utilities Totals	$3,095,419	$3,290,462	$4,751,826
								TOTALS	**$42,383,792**	**$45,545,771**	**$84,359,968**

Appendix A 14. Fixed operating costs associated with the hydrothermal liquefaction system. The costs are shown in 2018 $ and the results are representative of the Santa Monica, CA Bay HUC8 subbasin with a US maximum annual productivity of 25 g m^{-2} day^{-1}.

Labor	**Jones et al. (2014)** [17] **& Chen et al. (2021)** [18]				
Position	**Number**	**Salary (2014 $)**		**Position cost (2018 $)**	
Plant manager	1	$	150,000	$	157,030
Plant engineer	2	$	70,000	$	146,561
Maintenance supervisor	1	$	60,000	$	62,812
Lab manager	1	$	60,000	$	62,812
Shift supervisor	2	$	48,000	$	100,499
Lab tech	2	$	40,000	$	83,749
Maintenance tech	5	$	40,000	$	209,373
Shift operator	9	$	48,000	$	452,246
Yard employee	2	$	27,500	$	57,578
Clerks & secretaries	2	$	40,000	$	83,749
			Total Salaries	**$**	**1,416,411**
Other Fixed Costs					
Benefits + Overhead	90%	% of total salaries		$	1,274,770
Maintenance	3%	% of ISBL		$	2,530,799
Property Insurance	1%	% of FCI		$	1,585,967
			Total Fixed Costs	**$**	**1,416,411**

Appendix A 15. Variable operating costs associated with the hydrothermal liquefaction system. The costs are shown in 2018 $ and the results are representative of the Santa Monica Bay, CA HUC8 subbasin with a US maximum annual productivity of 25 g m^{-2} day^{-1}.

Variable	**Value**	**Units**	**Source**
Electricity	$0.036	$ kWh^{-1}	[15]
Catalyst	$38.90	$ kg^{-1}	[18]
Natural gas	$4.14	$ $MMBtu^{-1}$	[19]
Cooling water	$0.000227	$ kg^{-1}	[20]
Hydrogen	$ 1.39	$ kg^{-1}	[21]
Wastewater	$0.0054	$ gal^{-1}	[22]
Solids disposal	$0.029	$ kg^{-1}	[23]

8. Bibliography

[1] O.M. Daniel Wise, David Anning, David, Spatially referenced models of streamflow and nitrogen, phosphorus, and suspended-sediment transport in streams of the southwestern United States, 2019. https://doi.org/https://doi.org/10.3133/sir20195106.

[2] S.W. Ator, Spatially Referenced Models of Streamflow and Nitrogen, Phosphorus, and Suspended- Sediment Loads in Streams of the Northeastern United States, Sci. Investig. Rep. 2019-5118. (2019) 57. https://pubs.er.usgs.gov/publication/sir20195118.

[3] D.S. Dale Robertson, Spatially referenced models of streamflow and nitrogen, phosphorus, and suspended-sediment loads in streams of the Midwestern United States, 2019. https://doi.org/https://doi.org/10.3133/sir20195114.

[4] D. Wise, Spatially referenced models of streamflow and nitrogen, phosphorus, and suspended-sediment loads in streams of the Pacific region of the United States, 2019. https://doi.org/https://doi.org/10.3133/sir20195112.

[5] V.R.I. Anne Hoos, Spatially referenced models of streamflow and nitrogen, phosphorus, and suspended-sediment loads in the Southeastern United States, 2019. https://doi.org/https://doi.org/10.3133/sir20195135.

[6] J.M. Greene, D. Quiroz, S. Compton, P.J. Lammers, J.C. Quinn, A validated thermal and biological model for predicting algal productivity in large scale outdoor cultivation systems, Algal Res. 54 (2021) 102224. https://doi.org/10.1016/j.algal.2021.102224.

[7] C. Goldstein, Algae Energy Costs, Stanford Univ. (2011). http://large.stanford.edu/courses/2011/ph240/goldenstein1/#:~:text=The Reality of Algae&text=Algae based fuels remain an,significant obstacles must be considered.&text=Even after passing algae through,H2O by weight.

[8] S. Kim, C. Quiroz-Arita, E.A. Monroe, A. Siccardi, J. Mitchell, N. Huysman, R.W. Davis, Application of attached algae flow-ways for coupling biomass production with the utilization of dilute non-point source nutrients in the Upper Laguna Madre, TX, Water Res. 191 (2021) 116816. https://doi.org/10.1016/j.watres.2021.116816.

[9] S. Wilcox, W. Marion, Users manual for TMY3 data sets, Renew. Energy. (2008) 51. http://scholar.google.com/scholar?hl=en&btnG=Search&q=intitle:Users+Manual+for+TMY3+Data+Sets+Users+Manual+for+TMY3+Data+Sets#1%5Cnhttp://scholar.google.com/scholar?hl=en&btnG=Search&q=intitle:May.?Users+manual+for+TMY3+data+sets+users+manual+for+TMY3+dat.

[10] Uc. Argonne, GREET 1, (2021). https://greet.es.anl.gov/.

[11] G. Wernet, C. Bauer, B. Steubing, J. Reinhard, E. Moreno-Ruiz, B. Weidema, The ecoinvent database version 3 (part I): overview and methodology, Int. J. Life Cycle Assess. 21 (2016) 1218–1230. https://doi.org/10.1007/s11367-016-1087-8.

[12] Heijungs, Reinout., & Guinée, J. B. (1992). Environmental life cycle assessment of products. Centre of Environmental Science.

[13] K.K. DeRose, R.W. Davis, E.A. Monroe, J.C. Quinn, Economic viability of proactive

harmful algal bloom mitigation through attached algal growth, J. Great Lakes Res. 47 (2021) 1021–1032. https://doi.org/10.1016/j.jglr.2021.04.011.

[14] USDA, Land Values 2021 Summary, (2021). https://www.nass.usda.gov/Publications/Todays_Reports/reports/land0821.pdf.

[15] Eia, Wholesale Electricity and Natural Gas Market Data, U.S. Energy Inf. Adm. (2022). https://www.eia.gov/electricity/wholesale/#history.

[16] D. Knorr, J. Lukas, P. Schoen, Production of Advanced Biofuels via Liquefaction. Hydrothermal Liquefaction Reactor Design, Contract. 303 (2013) 275–3000.

[17] S. Jones, Y. Zhu, D. Anderson, R.T. Hallen, D.C. Elliott, Process Design and Economics for the Conversion of Algal Biomass to Hydrocarbons : Whole Algae Hydrothermal Liquefaction and Upgrading, Pnnl. (2014) 1–69. http://www.pnnl.gov/main/publications/external/technical_reports/PNNL-23227.pdf.

[18] P.H. Chen, J.L. Venegas Jimenez, S.M. Rowland, J.C. Quinn, L.M.L. Laurens, Nutrient recycle from algae hydrothermal liquefaction aqueous phase through a novel selective remediation approach, Algal Res. 46 (2020) 101776. https://doi.org/10.1016/j.algal.2019.101776.

[19] Eia, Natural Gas Summary, U.S. Energy Inf. Adm. (2022). https://www.eia.gov/dnav/ng/ng_sum_lsum_a_EPG0_PIN_DMcf_a.htm.

[20] D. Humbird, R. Davis, L. Tao, C. Kinchin, D. Hsu, A. Aden, P. Schoen, J. Lukas, B. Olthof, M. Worley, D. Sexton, D. Dudgeon, Process design and economics for conversion of lignocellulosic biomass to ethanol, NREL Tech. Rep. NREL/TP-5100-51400. 303 (2011) 275–3000. http://www.nrel.gov/docs/fy11osti/51400.pdf%5Cnpapers2://publication/uuid/49A5007E-9A58-4E2B-AB4E-4A4428F6EA66.

[21] Hydrogen In The Energy System: Focus On Production, Energy Innov. Policy Technol. LLC. (2018). https://energyinnovation.org/2018/04/02/hydrogen-in-the-energy-system-focus-on-production/.

[22] Rates and Fees, City Longmont. (2020). https://www.longmontcolorado.gov/departments/departments-n-z/water/rates-and-fees.

[23] R. Davis, C. Kinchin, J. Markham, E.C.D. Tan, L.M.L. Laurens, Process Design and Economics for the Conversion of Algal Biomass to Biofuels : Algal Biomass Fractionation to Lipid- Products Process Design and Economics for the Conversion of Algal Biomass to Biofuels : Algal Biomass Fractionation to Lipid- and Carbohyd, Nrel. (2014) NREL/TP-5100-62368.